Evolution of mushroom body inversion and associated gyriform neuropils parallel the evolved transposition of the mammalian hippocampus.

Nicholas James Strausfeld[1], Marcel Ethan Sayre[2]

[1]Department of Neuroscience, School of Mind, Brain and Behavior, University of Arizona, Tucson, United States; [2]Lund Vision Group, Department of Biology, Lund University, Lund, Sweden

Abstract

Neural organization of mushroom bodies (MB) is largely consistent across insects, whereas across malacostracan crustaceans the ancestral ground pattern diverges broadly, resulting in successive loss of lobes and acquisition of domed MBs retaining ancestral Hebbian-like networks and aminergic connections. We demonstrate here a radical departure from this evolutionary trend in the recent malacostracan lineage Brachyura. In the shore crab, *Hemigrapsus nudus*, MBs are entirely inverted. Instead of their expected location at the brain's rostral surface, inverted calyces are buried deep within it, extending columns (lobes) outwards to an expansive system of cortex-like gyri. This elaborate ensemble is DC0-immunoreactive, indicating extensive circuits for cognition. MB inversion and association with overlying gyri is an evolutionary novelty comparable to transposition of mammalian hippocampus to a location beneath multistratified cortices. We propose the brachyuran's unique MB and its associated gyriform centers have enabled its successful exploitation of topographically challenging habitats in water and on land.

Introduction

Insect mushroom bodies, particularly those of *Drosophila*, are the most accessible models for elucidating molecular and computational algorithms underlying learning and memory within genetically and connectomically defined circuits (e.g., Aso et al., 2014; Senapati et al., 2019; Modi et al., 2020; Jacob and Waddell, 2020). Another advantage of *Drosophila* is that it exemplifies a ground pattern organization that is largely consistent across hexapod lineages. These include Odonata (dragonflies), Dictyoptera (cockroaches), Lepidoptera (butterflies and moths), and Hymenoptera (wasps, honeybees, ants) (Ito et al., 1998, 2014; Sinakevitch et al., 2001; Li and Strausfeld, 1997; Montgomery and Ott 2015; Groh and Rössler, 2011). Because of the importance of mushroom bodies in understanding the relevance of synaptic organization in

sentience and cognition, recognizing evolutionary divergence of these centers would be expected to yield experimentally testable predictions about evolved modifications of circuitry in relation to ecological demands imposed on the species. However, insect mushroom bodies show a remarkably conserved organization, which makes them relatively unsuited for neuroevolutionary studies. There are some minor exceptions, to be sure: in honey bees and ants, calycal domains receive modality-specific afferents; in beetles, dietary generalists have more elaborate calyces than dietary specialists; in certain aquatic beetles there has been a modality switch from olfactory input to an exclusively visual input to the calyces (Gronenberg, 2001; Farris and Schulmeister, 2011; Lin and Strausfeld, 2012). Less attention has been given to other levels at which mushroom body organization may vary, such as neural arrangements comprising the mushroom body lobes (columns) and their outputs, although some studies have addressed organizational distinctions in basal groups such as silverfish (Zygentoma), dragonflies and mayflies (Farris,2005; Strausfeld et al., 2009).

The evolutionary stability of the insect mushroom body contrasts with the recent demonstration that mushroom bodies of malacostracan crustaceans have undergone substantial and often dramatic modification of the mandibulate (ancestral) mushroom body ground pattern (Stegner and Richter, 2011; Wolff et al., 2015, 2017; Strausfeld et al., 2020). Whereas Stomatopoda (mantis shrimps), the sister group of Eumalacostraca, possesses mushroom bodies like those of insects, equipped with calyces from which arise prominent columns (Wolff et al., 2017), the trend over geological time has been a reduction of those columnar components such that the ancestral ground pattern organization of parallel fibers and orthogonal Hebbian networks has become planar arrangements within domed centers lacking columns (Wolff et al., 2015; Strausfeld and Sayre, 2019; Strausfeld et al., 2020). These anatomical adaptations nevertheless share the property with the mushroom bodies of other arthropods of being immunopositive to an antibody raised against the catalytic subunit of protein kinase A, encoded by the *Drosophila* gene DC0, that is required for effective learning and memory (Kalderon and Rubin, 1988; Skoulakis et al., 1993). Antibodies raised against DC0 are reliable identifiers of neuropils mediating learning and memory both in arthropods and other phyla (Wolff and Strausfeld, 2012, 2015).

Whereas the evolutionary shift from columnar mushroom bodies to noncolumnar homologues is demonstrated across most decapod crustaceans, one lineage has defied unambiguous identification of a columnar or even a noncolumnar center. This is Brachyura, known in the vernacular as the crabs. Brachyura is a comparatively young lineage, recognized

58 from fossils dating from the mid-Jurassic (Schweizer and Feldmann, 2010; Guinot, 2019).
59 Phylogenomics places the origin of Brachyura also as mid-to-late Jurassic (Wolfe et al., 2019).
60 Brachyura is the most species-rich decapod clade, comprising 6,793 currently known species (Ng
61 et al., 2008). It is also a hugely successful lineage, extant species broadly distributed to occupy
62 benthic, littoral, estuarine, brackish, fresh water, terrestrial and even arboreal habitats. Many of
63 these ecologies are defined by complex topographies (Lee, 2015; Hartnell, 1988).
64 Historically, identifying a mushroom body homologue in the crab's brain has been
65 problematic. Claims for homologous centers range from paired neuropils in the brain's second
66 segment, the deutocerebrum, later attributed to the olfactory system (Bethe 1897), to an
67 insistence that the crab's reniform body is a mushroom body (Maza et al., 2016, 2020).
68 Demonstrated 132 years ago in stomatopod crustaceans, the reniform body is a morphologically
69 distinct center that coexists in the brain's lateral protocerebrum adjacent to its columnar
70 mushroom bodies (Bellonci, 1882; Thoen et al., 2019).
71 Until the present, observations of the varunid shore crab *Hemigrapsus nudus* have
72 identified large anti-DC0-reactive domains occupying almost the entire rostral volume of its
73 lateral protocerebrum but no evidence for mushroom bodies (Thoen et al., 2019). The affinity of
74 these domains to anti-DC0 suggested, therefore, a cognitive center far more expansive than
75 found in any other arthropod of comparable size, with the possible exception of the domed
76 mushroom body of the land hermit crab *Coenobita clypeatus* (Wolff et al., 2012). Here we
77 demonstrate that in the varunid crab there are indeed paired mushroom bodies. But these have
78 been "hiding in plain sight," having undergone a morphological transformation that is opposite to
79 the evolutionary trend towards a domed noncolumnar morphology, as in other reptantian
80 lineages. Here we present evidence of the unique disposition of the varunid mushroom body and
81 in the Discussion compare its organization to the evolved transformation of the ancestral planar
82 hippocampus (Hevner, 2016; Tosches et al., 2018).
83 In the varunid crab, paired mushroom bodies are inverted. Their calyces reside deep
84 within the lateral protocerebrum, a location that allows outward expansion of their columns,
85 which reach expanded cortex-like folds beneath the brain's surface. This orientation of the
86 varunid mushroom body is opposite to that in other pancrustaceans, in which the calyces are
87 situated under the rostral surface of the lateral protocerebrum with their columns extending
88 downwards into deeper neuropil (Strausfeld et al., 2009; Wolff et al., 2017; Sayre and
89 Strausfeld, 2018).

Characters (traits) defining the mushroom bodies of Stomatopoda correspond to those defining the mushroom bodies of *Drosophila* (Wolff et al., 2017). The following description of the varunid mushroom body uses complementary methods that resolve those traits in *Hemigrapsus nudus*. Reduced silver staining demonstrates spatial arrangements of calycal and columnar neuropils and their detailed neuroarchitecture. Osmium-ethyl gallate treatment of intact brains resolves neuronal densities; and serial sections of these preparations provide the three-dimensional reconstructions shown throughout this account (see Methods). Golgi mass-impregnations enable crucial insights into the exceptionally elaborate organization of varunid mushroom body intrinsic neurons, identified as the phenotypic homologues of insect Kenyon cells. Immunohistology has been used to resolve DC0-immunopositive components of the mushroom body calyces and columns, and antibodies raised against GAD (glutamic acid decarboxylase) reveal putative levels of local inhibition. Antibodies raised against tyrosine hydroxylase (TH) and 5-hydroxytryptophan (5HT) demonstrate arborizations consistent with those of output and input neurons intersecting different levels of the *Drosophila* and Stomatopod mushroom body columns.

We show that despite the varunid mushroom body's unparalleled intricacy and its unique transformation of the ancestral ground pattern, its defining traits demonstrate phenotypic homology with the mushroom bodies of insects and other crustaceans. We close with a Discussion proposing that the evolution of such intricacy, and the expansion of the lateral protocerebrum to accommodate mushroom body enlargement, is likely to have contributed novel circuits and, ultimately, to cognitive flexibility permitting certain Brachyura to exploit complex ecological topographies both on land and in the water.

Results

The Results are organized into eight sections, the first describing the overall location and structure of the varunid mushroom body. This is followed by the identification of its neural components and their arrangements as elaborate networks comprising the paired calyces. Descriptions of the internal organization of the calyces' rostral extensions, and their two prominent columns, culminates with an explanation of the cortex-like organization of overlying gyri to which the columns project. The final observations address the relationship of the mushroom body to the reniform body, a center common to malacostracan crustaceans. To

provide a three-dimensional understanding of this highly intricate system, descriptions refer to locations and arrangements within a reconstructed lateral protocerebrum and its major components (*see Methods*).

1. The varunid lateral protocerebrum (*Figures 1, 2, Figure 1 - figure supplement 1*)

In crabs, as is typical of stomatopods and most decapod crustaceans, the most anterior part of its brain, the protocerebrum, is flanked each side by a lateral outgrowth that expands into an enlargement of the eyestalk immediately proximal to the compound retina (*Figure 1 - figure supplement 1A*). This volume of brain comprises the lateral protocerebrum (*Figures 1A, 2A*). The lateral protocerebrum is connected to the midbrain proper by the eyestalk nerve composed of axons relaying information to and from the midbrain.

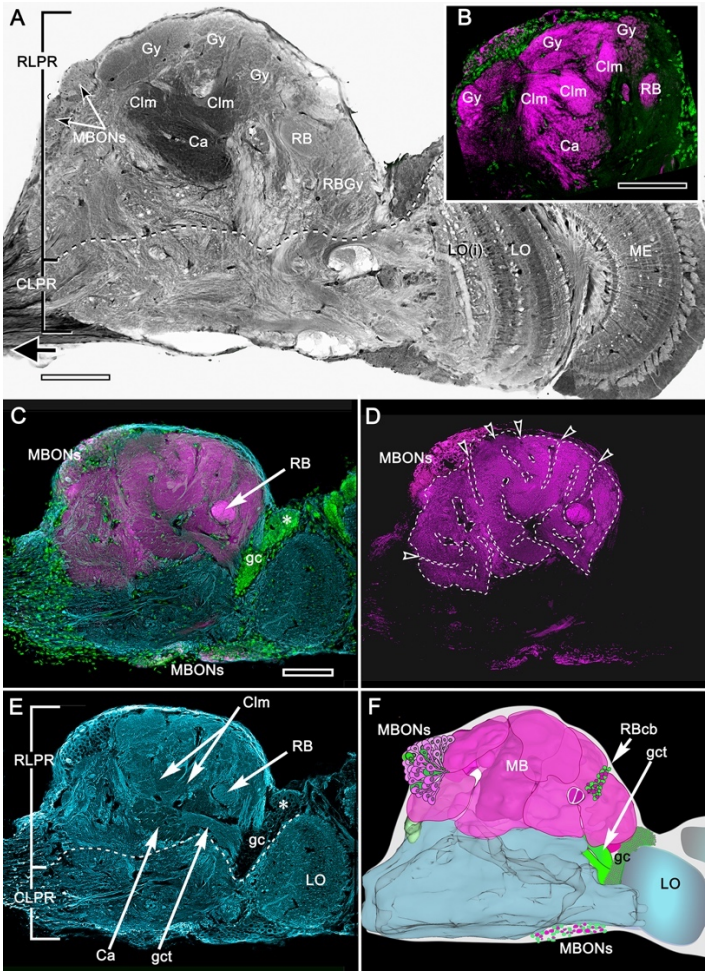

Figure 1. Organization of the varunid crab mushroom body and its associated gyri. (**A**) Brains treated with osmium-ethyl gallate demonstrate the overall disposition of neuropils, exemplified by this section of the lateral protocerebrum from its medial border to the optic lobe medulla. Its rostral domain (RLPR) includes

the mushroom body calyces (Ca), columns (Clm) and their associated gyriform neuropils (Gy).Clusters of neuronal cell bodies (here MBONs) are distributed over the neuropil. Distal volumes of the RLPR are associated with the reniform body (RB; here its pedestal and a gyrus RBGy), which is situated between the mushroom body and the optic lobe, here represented by its medulla (ME) and bilayered lobula (LO, LOi). The optic lobe provides outputs to discrete neuropils comprising the caudal lateral protocerebrum (CLPR). (**B-E**) Anti-DC0-labelled (magenta) volumes in panel B match the corresponding membrane-dense calyces and columns and their rostral gyri in panel A. Panel C demonstrates that DC0-immunostained gyri occupy almost the entire rostral level of the RLPR. Two small clusters caudally (MBONs) lining the CLPR, near the optic lobes, also include DC0-immunoreactive perikarya. The nuclear stain Syto13 (green) demonstrates the location of mushroom body globuli cells (gc) lying immediately beneath a group slightly large perikarya (asterisk). In panel D, removal of anti-□ tubulin and Syto13 labelling from C resolves the extent of the gyri and their many sulcus-like indentations (open arrowheads). In panel E anti-□□tubulin shown here alone resolves the overall fibroarchitecture of the LPR to provide correlative data with those provided by reduced silver stains (*Figure 2*). (**F**) Total Amira-generated reconstruction of a serial-sectioned, osmium-ethyl gallate treated eyestalk demonstrates the huge area of the lateral protocerebrum occupied by the folded gyri. Superimposed are the locations of small neurons supplying the reniform body (RBcb), mushroom body globuli cells (gc) and their tract of neurites leading to the calyx (gct), here obscured by overlying gyri. Scale bars, A, B, 100μm; C-F, 100μm.

Figure 1 —— figure supplement 1. Schematic of the *Hemigrapsus* brain

Brains treated with osmium-ethyl gallate or with reduced silver (*Figures 1A, 2A*) resolve the varunid lateral protocerebrum as a hump-shaped volume divided into a rostral and caudal part. The rostral lateral protocerebrum (RLPR), once referred to as the terminal medulla, a now defunct term (Strausfeld, 2020), is dominated by two centers: the mushroom bodies and the smaller reniform body. There is a small number of other satellite neuropils near the origin of the eyestalk nerve. The mushroom body is immediately recognizable by its intensely osmiophilic calyces from which arise columns that extend outwards, branching into a cortex-like neuropil composed of gyri (*Figure 1A*). These occupy the outermost volume of the RLPR. The reniform body comprises an independent system of interconnected neuropils situated laterally constrained to a volume of the RLPR that extends from its dorsal to its ventral surface (Thoen et al., 2019). In longitudinal sections of the RLPR, its prominent axon bundle, the pedestal, is seen in cross section(*Figures 1A, 2A*).

As in stomatopods and decapods, the crab's RLPR receives terminals of olfactory projection neurons originating from both the ipsi- and contralateral olfactory (antennular) lobes located in the brain's second segment, the deutocerebrum (*Figure 1 - figure supplement 1A, B*). The axons of more than a thousand projection neurons are organized into several discrete fascicles bundled together to provide the antennoglomerular tract (AGT). The left and right AGTs extend superficially across the midbrain to meet just dorsal to the central body. There, each tract bifurcates to provide inputs to each lateral protocerebrum from both the ipsi- and contralateral olfactory lobes (*Figure 1 - figure supplement 1A, B*). The eyestalk nerve also carries

176 other efferent axons to the lateral protocerebrum: these include relay neurons from other sensory
177 neuropils, relays from the opposite lateral protocerebrum and optic lobes, and interneurons
178 relaying from various midbrain neuropils.
179 The caudal volume of the lateral protocerebrum (CLPR) is mainly associated with
180 outputs from the optic lobe neuropils (*Figure 1A - figure supplement 1C*). Most of these originate
181 from the lobula, each bundle of outgoing axons representing a population of one of the numerous
182 morphological types of columnar neurons. Bundles segregate to a system of interconnected
183 neuropils called optic glomeruli, as occurs in insects (Okamura and Strausfeld, 2007). Further
184 relays from the glomeruli send information centrally to the midbrain via the eyestalk nerve. The
185 nerve also carries to the midbrain the axons of neurons from the lateral protocerebrum's rostral
186 neuropil, the mushroom bodies, and its associated gyri and from CLPR neuropils associated with
187 the optic glomeruli.
188
189 **2. Organization of DC0-positive volumes (*Figure 1*).**
190 The dense osmiophilic calyces and their extended columns (*Figure 1A*) correspond to discrete
191 neuropils showing high levels of immunoreactivity to antibodies raised against DC0 (*Figure 1B*).
192 The fibroarchitecture of these DC0-positive volumes is revealed by labeling with antibodies
193 against a-tubulin or by reduced silver. (*Figures 1E; 2A-C*) that provide correlative data for
194 resolving and interpreting the arrangements of the mushroom body volumes in 3-D
195 reconstructions (*Figure 2 - figure supplement 2*: see Methods). Salient both in osmium–ethyl
196 gallate-stained brains is the layer of gyri that defines the outer level of the rostral lateral
197 protocerebrum (*Figures 1A, 2D, E*). Gyri are DC0-immunoreactive and are contiguous with each
198 of the DC0-immunoreactive columns that extend outwards from the calyces. Gyri are resolved as
199 pillowed folds and indentations (sulci: *Figure 1D, F*) comparable to the folded architecture of a
200 mammalian cerebral cortex. This feature appears to be unique to Brachyura (see Discussion).
201
202 **3. The calyces and their origin from globuli cells (*Figures 1, 2*)**
203 If centers are claimed as phenotypic homologues of insect mushroom bodies, then the centers are
204 expected to have the following categories of neurons irrespective of their divergence from the
205 ancestral ground pattern as represented in the allotriocarid clade Cephalocarida (Stegner and
206 Richter, 2011). These categories are: 1) intrinsic neurons, the most populous of which are
207 Kenyon cells defining the mushroom body's volume, shape, and subdivisions; 2) extrinsic

208 neurons providing inputs from sensory centers (Kanzaki et al., 1989; Lin and Strausfeld, 2012;
209 Li et al., 2020), as well as protocerebral regions encoding high level multisensory information
210 (Li and Strausfeld, 1999); and 3) output neurons that encode information computed by levels of
211 the mushroom body lobes (Li and Strausfeld, 1999; Turner et al., 2008). The latter are referred to
212 here as MBONs, adopting the term from studies on *Drosophila* (Aso et al., 2014a,b).

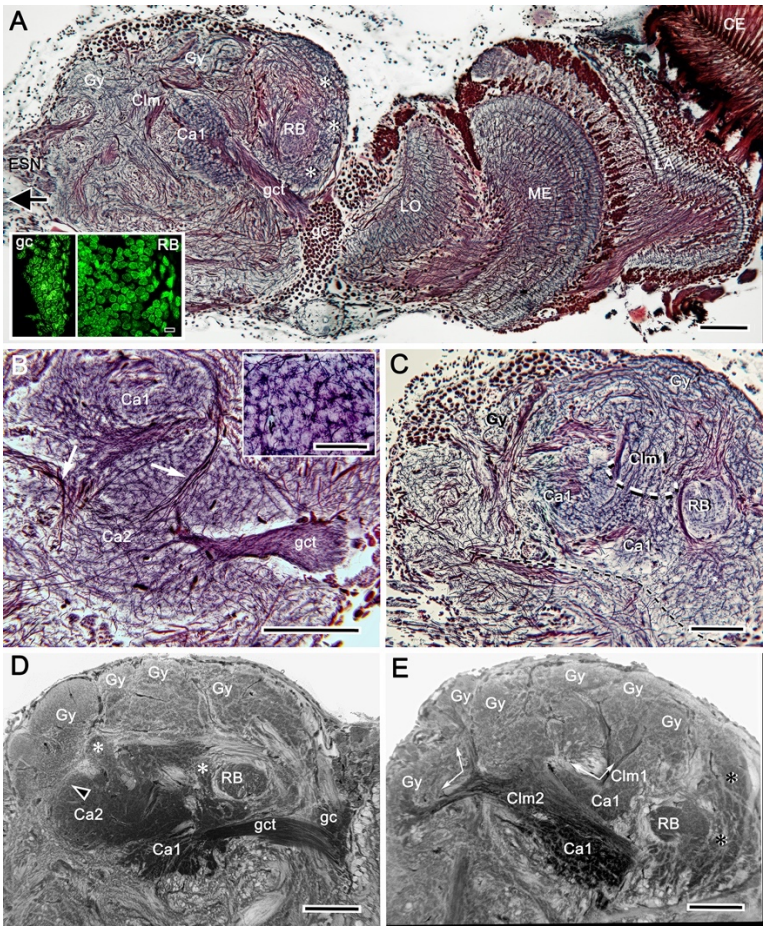

213

214 **Figure 2.** Uniquely identifiable neuropils of the mushroom bodies are resolved by reduced silver. (**A**)
215 Horizontal section of the lateral protocerebrum demonstrating the more dorsal of the two calyces (Ca1)
216 and its supply by the globuli cell tract (gct) from the cluster of globuli cells (gc). Columnar extensions
217 (Clm) from the calyces reach out to overlying gyri (Gy). The reniform body is shown with three of its gyri
218 (asterisks) and its bundled axons (RB) situated between the mushroom body and optic lobes, insets lower
219 left compare the smallest perikarya supplying the calyces (globuli cells, gc) with the next smallest
220 perikarya belonging to neurons of the reniform body (see *Figure 2 -figure supplement 1*). Abbreviations:
221 ESN, eyestalk nerve; CE, compound retina, LA, lamina, ME, medulla; LO, lobula. (**B**) Adjacent calyces
222 (Ca1, Ca2) showing their diagnostic arrangement of microglomeruli (inset upper right; see also Figure 3).
223 Arrows indicate afferent fibers into Ca2 from nonolfactory origins. (**C**) The calycal origin and rostral
224 extension of the Ca1 column (encircled). At this level, penetration by en passant axon bundles causes the
225 calyx to appear fragmented. (**D, E**) Osmium ethyl gallate-treated sections at two depths. Panel D
226 indicates the bulk and elaboration of calycal neuropils. At this level calyx 2 appears as the larger. The
227 arrowhead indicates the root of column 2. Calyx 1 is shown with its globuli cell tract entering a domain
228 denoted by lateral extensions of calyx 1. In panel E, the base of column 1 (Clm1) is shown arising from

Ca1, its curvature at this level splitting it into two parts. Column (Clm2) is shown extending two branches into the gyriform layer above. Clm1 extends outwards just proximal to the pedestal of the reniform body (RB). In addition to columns, calyces provide occasional narrower finger-like extensions extending towards the gyri (asterisks in D). Scale bars, 100μm. Inset in A, 10μm, inset in B, 50μm.
Figure 2 —— figure supplement 1. Globuli cells supplying intrinsic neuron to the mushroom bodies
Figure 2 —— figure supplement 2. Globuli cells provide two tracts, one to each calyx.

Intrinsic neurons supplying the *Hemigrapsus nudus* calyces correspond to insect Kenyon cells. As do insect Kenyon cells, these originate from the brain's smallest and most crowded population of neuronal cell bodies, the globuli cells (*Figures 1C, 2A,D, Figure 2 – figure supplement 1*). In other arthropods globuli cell perikarya have been shown as dense clusters situated at the rostral surface of the lateral protocerebrum, usually near its proximal margin or immediately above the mushroom body calyces, as in *Drosophila* or Stomatopoda, or, in malacostracans with eyestalks, close to the lateral protocerebrum's attachment to the eyestalk nerve. In *H. nudus*, however, globuli cell perikarya are found in a completely different and surprising locality: a densely populated "hidden" volume tucked between the proximal margin of the lobula and the most distal border of the lateral protocerebrum (*Figure 2A*). As in other pancrustaceans these perikarya are the smallest perikarya of the brain, in the varunid ranging from 5 to 7 μm in diameter (compared in *Figure 2A, inset, Figure 2 – figure supplement 1*). In crabs used for these studies (carapace widths of 4-8 cm), we estimate that this perikaryal cluster accounts for 22,000 mushroom body intrinsic neurons shared by the two calyces (see Methods). Cytological distinctions amongst cells in the cluster, denoted by their appearance after osmium-ethyl gallate staining (Wigglesworth, 1957), suggest that new globuli cells are being continuously generated from ganglion mother cells situated at the cluster's periphery (*Figure 2 - figure supplement 1D-G*).

Cell body fibers (neurites) extending from the globuli cell cluster are tightly packed into two prominent bundles, called globuli cell tracts, one projecting obliquely ventrally the other obliquely dorsally to supply each of the two adjacent calyces (*Figure 2A, B, D - figure supplement 2*). Neurites comprising these tracts fan out to supply each calyx with its ensembles of mostly orthogonally arranged dendritic networks that interweave amongst a mosaic of microglomeruli (*Figure 2B; Figure 3A, B, - figure supplement 1*). The networks, which are resolved by silver stains, comprise overlapping populations of intrinsic neuron processes extending amongst a mosaic of many thousands of discrete microglomeruli (*Figures 2B, 3A*). These are assumed to be sites of synaptic convergence (*Figure 3- figure supplement 1*),

263 corresponding to microglomerular organization in the calyces of insect, stomatopod and caridean
264 mushroom bodies (Groh and Rössler, 2011;) Wolff et al., 2017; Sayre and Strausfeld, 2019. As
265 will be described in the following section, components of microglomeruli include the terminals
266 of afferent relays originating from the olfactory lobes, neuropils associated with the visual
267 system, including the reniform body, and centrifugal neurons from the midbrain.
268 Serial sections oriented horizontally, approximately parallel to the rostral surface of the
269 protocerebrum and stained with reduced silver, suggest the calyces are planar neuropils (*Figure*
270 *2B*). But this is deceptive, as shown by sections in the vertical plane demonstrating how the deep
271 calycal cytoarchitecture extends rostrally to merge with the base of its column(*Figure 2C*). The
272 total extent and volume of calycal neuropil is surprisingly large as can be seen in intact brains
273 treated with osmium-ethyl gallate, a technique that selectively colors cell membranes black
274 (Wigglesworth, 1957). The method reveals volumes of neuropil in shades of black to light gray,
275 the darker the neuropil, the more densely packed its neuronal processes (*Figures 1A, 2D, E;*
276 *Figure 4A, figure supplement 1*). This density is a reflection of the many thousands of intrinsic
277 neurons comprising the calyces. Volumes that are paler are composed of neuronal processes that
278 are stouter and contribute less stainable membrane, as in the overlying gyri.
279 Computer-generated reconstructions and rotations of osmium-ethyl gallate stained
280 sections (see Methods) demonstrate that the calycal volumes are topographically elaborate
281 (*Figure 2 supplement 2*); each calyx is stratified at deeper levels of the lateral protocerebrum's
282 rostral volume, but where calycal neuropils extend rostrally their upper borders are defined by
283 irregular arrangements of small peaks and troughs. Two prominent columns, one from each
284 calyx, extend outwards into the overlying gyri (*Figure 2E*). Reduced silver material and Golgi
285 impregnations resolve their elaborate internal organization (*Figure 2C*), which is described in
286 section 5, below.
287
288 **4. Neuronal organization of the calyces (Figures 3-6)**
289 Intrinsic neuron processes comprise the varunid calyces (*Figure 3B, Figure 3 - figure supplement*
290 *1; Figure 4B-G, Figure 4 - figure supplement 1*). They receive inputs from neurons primarily
291 from the deutocerebrum (*Figure 3 – figure supplement 1B*) but also from the optic lobes and
292 from its associated neuropils, such as the reniform body (*Figure 4 - figure supplement 2*), as also
293 shown for Stomatopoda (Thoen et al., 2019). Golgi impregnations and osmium-ethyl gallate
294 stainings demonstrate that calyces, across their horizontal and vertical extent, are composed of

295 discrete domains of morphologically distinct networks comparable to the discrete modality-
296 specific zones of Kenyon cell dendrites that define the insect calyces (Ehmer and Gronenberg,
297 2002; Strausfeld, 2002).

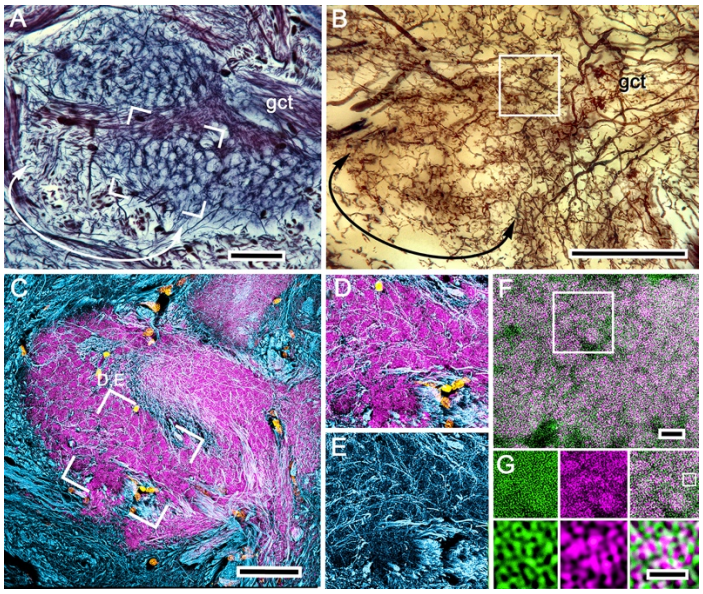

298

299 **Figure 3.** Organization of calyx 1: microglomeruli. (**A**) Reduced-silver-stained calyx showing its globuli cell
300 tract (gct) with, at a different level, many of its constituent neurites giving rise to branches that delineate the
301 mosaic organization of microglomeruli. (**B**) Golgi impregnations provide examples of intrinsic neurons, the
302 branches and fine processes of which extend through domains of the calyx that correspond to those
303 revealed both by reduced silver and by antibodies against DC0. A subfield (curved double arrow) in panel
304 A corresponds to the denoted branches of the illustrated intrinsic neuron in panel B. (**C**) Microglomeruli are
305 specifically labelled by anti-DC0. Microglomerular size and density in the boxed area corresponds to an
306 equivalent microglomerular organization identified by reduced silver (boxed areas in A). (**D-G**) The mosaic
307 is also reflected by the pattern of all intrinsic neuron processes at that level revealed by anti-α–tubulin;
308 these enwrap DC0-positive microglomeruli (D, E). The same system of microglomeruli is resolved using
309 combined actin/anti-synapsin. The area identified in a field of Golgi-impregnated intrinsic neuron processes
310 (boxed in B) is equivalent to the area of the calyx in panel F labelled with actin/anti-synapsin demonstrating
311 the microglomerular mosaic. The boxed area in F is shown in panel G. (**G**) The upper row shows actin and
312 synapsin separate, with the superimposed images in the right panel in G). The boxed area in the upper
313 right panel of G indicates a single microglomerulus. This is enlarged in the lower three panels of G, again
314 showing actin and synapsin as separate images and then combined lower right to demonstrate the density
315 of synapsin-labelled profiles, and thus direct evidence of massive convergence at a calycal microglomerulus
316 (panel G). Scale bars, A–C, 50μm; F, 10μm; G, 2μm.
317 **Figure 3 —— figure supplement 1.** Rectilinear network organization of the calyx and afferent supply.
318

319 Most calycal neuropil is characterized by its dense arrangement of small almond-shaped
320 subunits (*Figure 3A*), here referred to as microglomeruli following the term given to comparable
321 elements described from insect mushroom body calyces (Yasuyama et al., 2002 Sjöholm et al.,
322 2006; Groh and Rössler, 2011). However, peripheral volumes are limited to the more dorsal of
323 the two calyces, here referred to as calyx 1 (*Figure 3A, B*), comprise more distributed

arrangements (*Figure 3A,B*). These appear to receive terminals from axons of relay neurons emerging from fascicles in the eyestalk nerve that are not part of projections from the olfactory lobes.

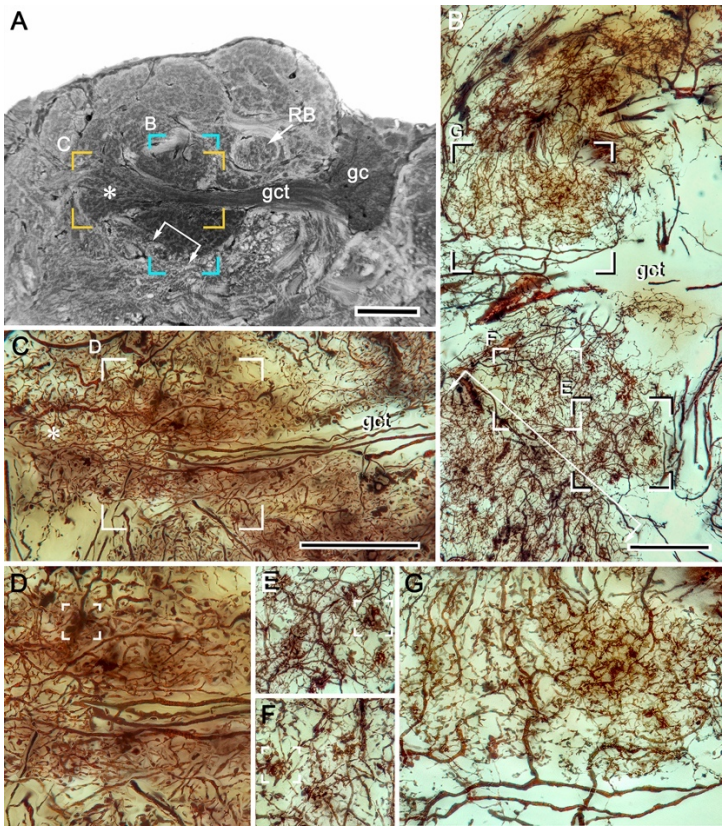

Figure 4. Intrinsic cell dendrites define calycal territories. (**A**) Osmium-ethyl gallate resolves calycal territories matching the dendritic fields of morphologically distinct intrinsic neurons. Letters in panel A indicate panels showing corresponding locations of Golgi-impregnate dendritic fields shown in B and C. Boxed areas in B and C are enlarged in panels D–G to demonstrate distinctive dendritic morphologies. The locations of the arrowed bracket and asterisk in A correspond to their locations in B (the bracket) and C (the asterisk). These further indicate the fidelity of calyx organization indicated by these two histological methods. Open boxes in panels D–-F indicate different morphological specializations of afferent terminals. Abbreviations: RB, reniform pedestal; gc, globuli cells; gct, globuli cell tract. Scale bars, A, C, 100μm, B, 50μm.

Figure 4 —— figure supplement 1. Fidelity of intrinsic neurons fields

Figure 4 —— figure supplement 2. Calyx distinctions

Discrete fields comprising intrinsic cell processes are recognized by their distinctive and particular morphologies (*Figure 4B–G, Figure 4 – figure supplement 1*). Each morphological type is defined by the patterning of its initial branches from its globuli cell neurite and the subsequent patterns made by their tributaries down to the details of their final specializations. The latter indicate points of functional connection and are morphologically comparable to the

claws, clasps and dendritic spines that decorate the dendritic branches of Kenyon cells in *Drosophila* and other insects (Ito et al., 1998; Strausfeld and Li, 1999; Strausfeld 2002) and the dendrites of homologous intrinsic neurons in the mushroom bodies of marine hermit crabs (Strausfeld and Sayre, 2019). As in those taxa, in the varunid calyx these specializations invariably relate to the distribution and patterning of its microglomeruli (*Figure 3A,B*).

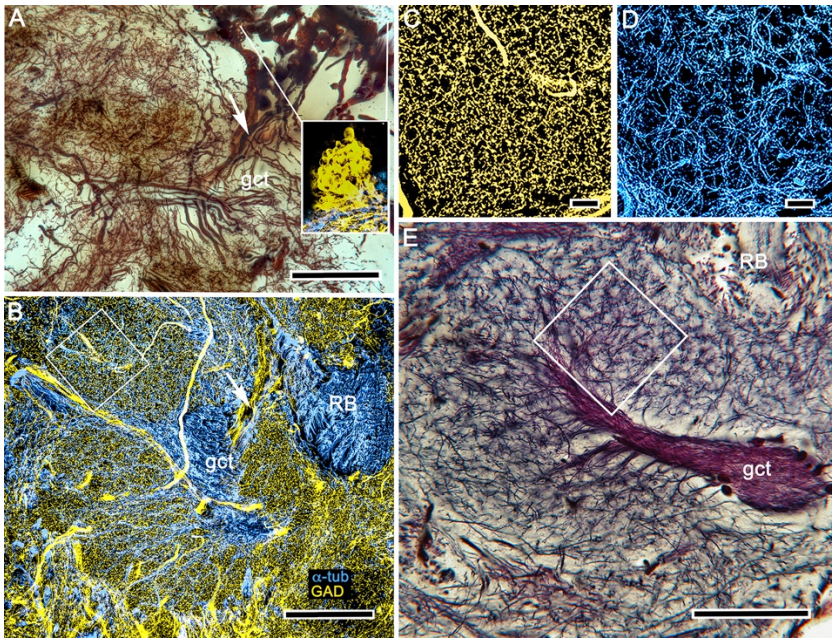

Figure 5. Evidence for local inhibition in the calyx by anaxonal neurons. (**A**) 40-50 large perikarya situated rostrally above the gyri are immunoreactive to glutamic acid decarboxylase (GAD, as shown in the right inset. These neuron cell bodies, which are here Golgi–impregnated, send stout cell body fibers (arrow) to the calyces where they provide widely branching and extremely dense processes that do not follow the patterns of the microglomerular mosaic. (**B**) GAD immunoreactivity reveals their branches and finest processes spreading through every calycal domain and hence positioned to potentially interact with all the intrinsic neuron dendritic fields. (**C, D**) GAD immunoreactivity in an area shown by the box in panel B, and an equivalent area in panel E showing the mosaic of microglomeruli. This mosaic is also evident from the pattern a α-tubulin-immunoreactive intrinsic neurons shown in D (same boxed area in B Scale bars, A, B, 100μm, C, D, 10μm, E, 50μm.

Microglomeruli as revealed by reduced silver are also highlighted by their intense immunoreactivity to antibodies raised against DC0. DC0-immunoreactive microglomeruli beautifully match silver-stained microglomeruli with respect to their size and packing (*Figure 3 A,C*). The bundled branches of intrinsic neurons resolved by antibodies against α-tubulin (*Figure 3D,E*) further resolve microglomeruli as participants of an elaborate organization of orthogonal

367 networks that correspond to distinct morphological types of intrinsic neurons revealed as single
368 cells by Golgi-impregnation (*Figure 4B,C, Figure 4 - figure supplement 1*). Each glomerulus
369 signifies the site of an incoming terminal's presynaptic bouton or varicosity (*Figure 3 - figure*
370 *supplement 1*). Combined anti-synapsin immunoreactivity and F-actin labelling (*Figure 3F-G*)
371 further demonstrates the profusion of postsynaptic sites belonging to intrinsic neurons that
372 converge at each microglomerulus. The densely packed presynaptic specializations further
373 confirm the status of a microglomerulus as the site of massive transfer of information from
374 presynaptic terminals onto many postsynaptic channels.

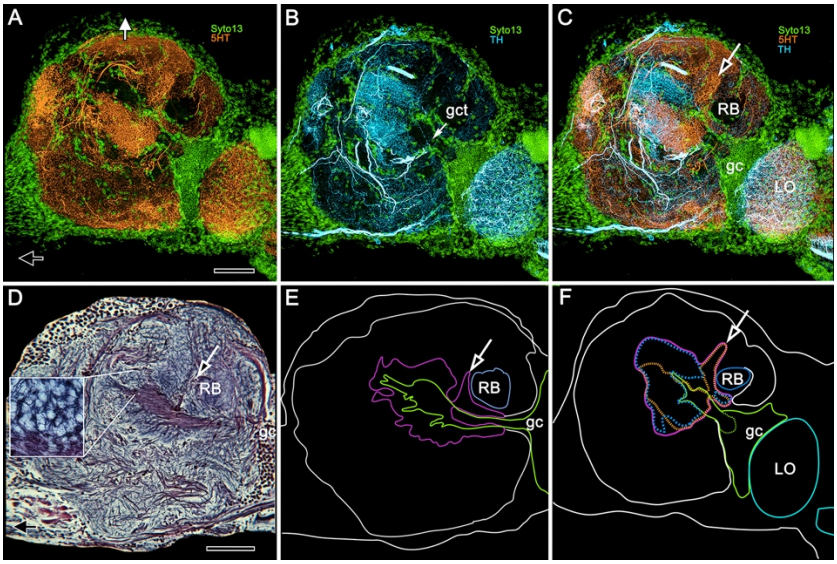

375

376 **Figure 6. 5HT and TH immunoreactivity define different calycal domains.** (**A,B**) Although many
377 volumes of the lateral protocerebrum are distinguished by 5HT (panel **A**, 5 hydroxytryptophan, orange)
378 immunoreactivity, the densest system of branches is in a rostral domain of calyx 1. TH (panel **B**, tyrosine
379 hydroxylase, cyan) defines two domains, one partially overlapping 5HT, the other not (panel **C**). (**D**) Bodian
380 silver-stained calyx 1 showing its distinctive microglomerular mosaic (inset). (**E**) Outlined in purple is the
381 total calycal perimeter at this level of sectioning and orientation. The open arrow indicates the origin of
382 column 1. (**F**) Perimeter (purple) of calyx 1 in a section of the RLPR slightly rotated around its lateral-medial
383 axis, mapping within it 5HT- and TH- immunoreactivity (as in panels A–C) also indicating the origin of
384 column 1 (open arrow, as in panel C). Abbreviations: RB, reniform body; gc, globuli cell cluster; gct, globuli
385 cell tract; LO, lobula. Scale bars for all panels, 100μm.
386

387 As remarked, the shapes and arrangements of intrinsic neurons and their synaptic
388 specializations contribute to orthogonal networks in the calyces and define calycal domains.
389 However, the domains are not arranged as neatly adjacent territories as in the insect calyx
390 (Gronenberg, 2001). Instead, the varunid calyx can reveal domains that extend vertically or
391 horizontally (*Figure 3 - figure supplement 1*), or comprise unexpectedly elaborate arrangements
392 that are understood only after they are matched to an appropriately oriented osmium-ethyl gallate

393 section (*Figure 4A,B, figure supplement 1*). One of the most challenging of these arrangements
394 consists of a population of intrinsic neurons defining a cylindrical domain that splays out as it
395 extends towards the proximal margin of the lateral protocerebrum (*Figure 4A*). The entire
396 ensemble comprises densely branched narrow-field arborizations that surround the initial
397 branches of a subset of globuli cell neurites (*Figure 4A,C,D*). The core leads to a terminal
398 expansion that is confluent with the base of one of the two large columns that extends to the
399 overlying gyri. Serial reduced-silver sections reveal this as originating only from calyx 2,
400 indicating that calyx 2 differs from calyx 1 with regard to at least one population of intrinsic
401 neurons. As in many insect lineages where there are paired calyces, it is such subtle distinctions
402 that demonstrate disparate organization across paired calyces (Farris and Strausfeld, 2003).
403 Reduced-silver stains showing axon tracts reveal inputs to calyx 2 originating from a tract
404 that recruits its axons from the reniform body and the medulla. Collaterals from this tract spread
405 into a deep level of calyx2 neuropil where they spread across microglomeruli bordering one side
406 of the incoming neurites from the globuli cell tract (*Figure 4 - figure supplement 2*). The
407 correspondence of this arrangement with insect calyces is considered below in the Discussion.
408 There is one critical exception to the generalization that calycal subdivisions are denoted
409 by different types of intrinsic neurons. The exception is that there is a system of neurons that
410 arborizes uniformly throughout both calyces. These arborizations belong to GAD-
411 immunoreactive local processes originating from a dorsal cluster of large cell bodies, each of
412 which provides an anaxonal field that arborizes throughout both calyces, and into each of its
413 domains. (*Figure 5A,B*). These densely packed processes are exceptional in that they do not obey
414 the orthogonal leitmotif of the calyx, as revealed by anti-a-tubulin (*Figure 5C, D*), nor do they
415 reflect the mosaic arrangement of glomeruli (Figure *5C-E*). Instead, anti-GAD-immunoreactive
416 branchlets populate all the calycal domains and do so in great numbers, the totality suggesting
417 that local inhibitory elements are distributed amongst all intrinsic cell processes irrespective of
418 whether they are in immediate proximity to or distant from a microglomerulus (*Figure 5 C-E*).
419 Whereas GAD immunohistology does not distinguish local calycal domains, these are
420 indicated by the inhomogeneity of fields of 5HT- and TH-immunoreactive across the calyces
421 (*Figure 6*). The neurons providing these fields also appear to be specific to the calyces and not
422 part of a wider system that extends to other regions of the LPR. Those more distributed systems
423 include densely branched arborizations that populate the optic lobe's lobula and 5HT-
424 immunoreactive neurons that arborize in certain neuropils of the CLPR as well as gyri. These are

likewise distinct from the 5HT and TH-immunoreactive fields that intersect the mushroom body columns, which are described next.

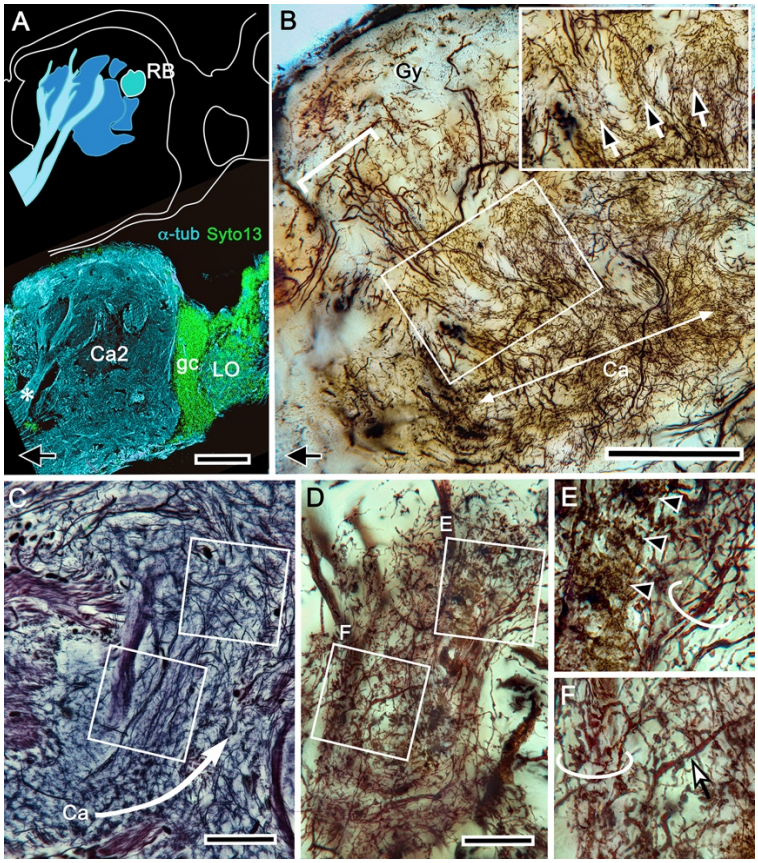

Figure 7. Origin of calycal extensions and columns. (**A, B**) Anti-α–tubulin (cyan) reveals the organization of large fiber bundles and coarse neuropil but, at low magnification, shows neuropils of the calyces as almost featureless (panel A). Part of the calyces are penetrated by incoming tributaries from the eyestalk nerve (asterisk in A, lower panel). A corresponding Golgi-impregnated region (B) demonstrates a system of medium-diameter branched processes that provide fine networks enwrapping the origin of columns. Some networks also extend as finger-like extensions outwards from the calyces. Panel B shows one column (upper left bracket) the base of which is flanked by those arrangements (enlarged in upper right inset indicated by arrows). This extensive system of processes does not derive from the globuli cell clusters although it is clearly associated with the entire extent of the calyces, suggesting a possible role in calyx-wide modulation. (**C-D**) As shown by this reduced silver stained section, the column arising from calyx 1 is extremely elaborate, comprising at least two longitudinal divisions each defined by arrangements of intrinsic neuron processes and their branched specializations. The curved arrow in panel C indicates the continuation of intrinsic neuron microglomeruli for a short distance alongside the column. The boxed areas in panel C, indicate corresponding levels identified in a Golgi-impregnated column 1 (D) showing enlargements in panels E, F, of their constituent arrangements. In panel E ascending fibers provide short collaterals (arrowheads) across one longitudinal subdivision of the column. In another subdivision, ascending intrinsic processes are arranged as a tangle (circled in panels E, F). Panel F also shows a large beaded branch (arrowed) of a mushroom body input neuron (MBIN) extending into the column. Abbreviations: RB, reniform body; Ca2, calyx 2; gc, globuli cells; LO, lobula; Gy, gyri. Scale bars, A, B, 100μm; C, D, 50μm.

Figure 7 —— figure supplement 1. Intrinsic neuron organization in columns

Figure 7 —— figure supplement 2. The interface between columns and gyri.

450 **5. Transition from the calyces to the columns**

451 Thus far we have demonstrated the composition of the calyces by approximately orthogonal
452 networks provided by intrinsic neurons and their arrangements with microglomeruli.

453 Stomatopod and shrimp mushroom bodies demonstrate a clear transition of neuronal
454 organization between the calyx and its columnar extensions (Wolff et al., 2017; Sayre and
455 Strausfeld, 2018). In *H. nudus* there is no abrupt transition (*Figure 2)*. This ambiguity is
456 seconded in brains treated with osmium-ethyl gallate, which show lateral protocerebral neuropil
457 supplied by globuli cell neurites gradually fading from black to gray, signifying decreasing
458 densities of neuronal membrane, finally giving way to the uniformly pale aspect of the overlying
459 gyri (*Figure 1A, Figure2D,E*). 3-D reconstructions of the dark volumes show a layered
460 arrangement at deeper layers of the calyces changing to a more corrugated appearance,
461 particularly at its outer surface (*Figure 2, supplement 2*). Silver impregnations show that the base
462 and some of the initial length of a column are clearly reticulated (*Figure 7C*). Double Golgi
463 impregnation shows that these networks receive contributions from two sources: the extensions
464 of axon-like processes from intrinsic neuron fields in the calyx; and intrinsic arborizations, many
465 extremely compicated, that originate from thin neurites, presumed to belong to globuli cells
466 (*Figure 7 - figure supplement 1*). An additional system of networks extends outwards to flank
467 each calyx's column (*Figure 7B*). These reticulations originate from a tangle of processes
468 situated at a deeper level of the calyces (*Figure 7B*) that does not reflect any relationships with
469 microglomeruli. The likely origin of this system (*Figure 7B*) is not from globuli cells but from a
470 small clusters of cell bodies, some DC0-immunoreactive, situated ventrally close the inner
471 margin of the lobula (*Figure 1C*). We interpret this tangle of processes (*Figure 7B*) as belonging
472 to interstitial local interneurons providing elements to the columns at a level limited to their
473 emergence from the calyces a small part of their initial length. The topology of these
474 arrangements, including the small column-specific intrisnic arborizations (*Figure 7 - figure*
475 *supplement 1E*-K) is reminiscent to that of interstitial neurons interposed between the calyces
476 and pedunculus of the honeybee (Strausfeld, 2002).

477 The origin of the columns and smaller extensions from the calyces are further
478 demonstrated by selected levels of silver-stained brains. Serial sections resolve the uneven rostral
479 border of the calyces and the two columns reaching outwards towards the overlying gyri (*Figure*
480 *7 - figure supplement 2*). The series also demonstrates the fidelity of silver and osmium-ethyl
481 gallate in showing corresponding origins of the columns from the two calyces. These aspects

482 emphasize that the seemingly irregular morphology of the rostral part of the calyces is not
483 irregular by happenstance but is a defining feature of the lateral protocerebrum.
484 Reduced silver preparations demonstrate that a column is subdivided into parallel
485 components as in insect mushroom bodies, where each subdivision has a distinctive arrangement
486 of intrinsic neurons (Strausfeld et al. 2005; Sjöholm et al., 2005; Tanaka et al., 2008) and is
487 defined by distinctive patterns of gene expression (Yang et al., 1995). What is unexpected is the
488 degree of elaboration observed in the varunid mushroom body. Golgi impregnations demonstrate
489 that, compared with other pancrustaceans, mushroom bodies in a crab are stunningly complex,
490 both with regard to their calyces and columns. The varunid's columns consist of parallel intrinsic
491 cell fibers that are almost obscured by numerous other arrangements, the variety of which is
492 compatible with the variety of their morphological fields in the calyces. Comparison of the
493 silver-stained column originating from calyx 2 to one impregnated by mass Golgi impregnations
494 (*Figure 7C,D*) demonstrates a discrete and complicated system of processes, some providing
495 bridgelike connections across them (*Figure 7E*), others having irregular branches, lateral
496 prolongations, and bundled parallel fibers (*Figure 7E,F*). In addition, larger dendrite-like
497 elements arising from stout processes within the columns suggest that those processes may
498 provide outputs extending outwards to the overlying gyri (*Figure 7D,F*), a feature to which we
499 return in section 7.
500 Golgi impregnation has its own peculiar limitations: it is stochastic, revealing probably
501 less than 1% of the total population of neurons, even after double impregnation. Nevertheless,
502 mass impregnation further suggests that the columns from the two calyces are not identical.
503 Although networks of intrinsic cells in both columns receive terminals from branches of the
504 olfactory glomerular tract, there are clear differences between the columns from calyx 1 and
505 calyx 2. Column 2 is broader and more difficult to discern in reduced silver. In part because
506 many of its intrinsic processes are all extremely thin, many less than a micron in diameter (see
507 section 7 below). At first sight, the organization of processes comprising column 2 appears to be
508 chaotic. However, when scrutinized more closely the organizations of its dendrites and
509 collaterals contribute to subsets of different arrangements disposed across the width of a column
510 and at different levels along it (*Figure 7 supplement 1A-C*). Reciprocal channels to the column
511 from the gyri are suggested by the presence of descending axons flanking the column, providing
512 varicose collaterals into it (*Figure 7 - figure supplement 1A*). These varieties of of columnar
513 arrangements are further considered in the Discussion.

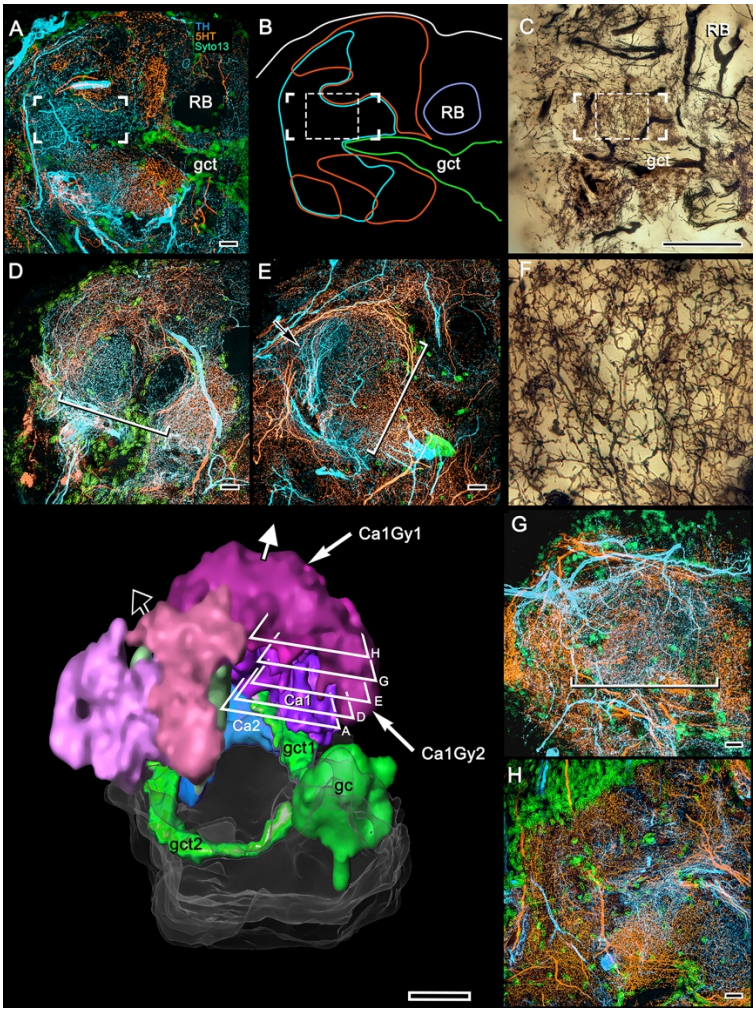

Figure 8. **5HT and TH immunoreactivity resolve different levels in the calyx 1 column.** Looking downwards through the rostral surface of LPR**,** this sequence of confocal slices (**A,D,E,G,H**) shows views starting at the column's origin from calyx 1 (panel **A**) then following its outward passage rostrally to the level at which the column merges with the overlying gyri (panels **G**, **H**). (**B)** shows outlines of 5HT- and TH-immunoreactive fields at level A in relation to the globuli cell tract (gct, green) and the cross section of the reniform body's pedestal (RB).The dendritic field of a TH-immunoreactive cell is bracketed in A,B and a smaller portion of it is denoted by a dashed square in B. (**C**) Golgi preparation of dendrites in area equivalent to bracketed and dashed areas in (B) show that at this level, networks of intrinsic neurons have given way to more loosely defined reticulations. (**F**) Enlargement of dashed square in (C). At the level shown in panel A, 5HT- and TH-immunoreactive fields are segregated across the origin of the column and continue to be, at least until the level shown in panel **E**, suggesting 5HT- and TH-immunoreactive fields are restricted to the column's longitudinal subdivisions. TH-immunoreactive fields can be noticeably clustered within a small area of the column's cross-section (arrow in E) as are MBONs in *Drosophila* mushroom bodies. The width of the column (brackets in panels D, E, G) increases gradually through layers **D**, **E**, and **G** (see brackets), and in the gyrus (**H**) its borders are no longer distinguishable. The 3–D reconstruction (lower left) shows a view looking into the lateral protocerebrum from its confluence with the optic lobes, its medial axis indicated by the black arrow and the rostral axis by the white arrow pointing upwards. Confocal levels are indicated as well as the two gyri (Ca1Gy1, Ca1Gy2) associated with the Ca1 column and the globuli cell tracts to Ca1 and Ca2 from the globuli cell cluster (gc). Other abbreviations: gct, globuli cell tract; pds, pedestal of the reniform body; Gy, gyrus. Scale bars, A-E, G, H, 10μm; C and 3–D reconstruction, 100μm.

536 Fields of 5HT- and TH-immunoreactive neurons extend across columns. Here we show
537 fields relating to column 1 from calyx 1 that provide clear resolution of their arrangements from
538 the calycal origin to the interface with gyri (*Figure 8*). Fields are arranged at specific levels
539 along the column and they intersect different domains across the column, as occurs across the
540 parallel subdivision of the columns (lobes) of mushroom bodies in *Drosophila* and other insects
541 (Nässel and Elekes 1992; Liu et al., 2012; Aso et al., 2014a; Hamanaka, 2016; Tedjakumala et
542 al., 2017;). The first of these fields occurs at the origin of the column from the calyx (*Figure*
543 *8A,B*) above where the neat orthogonal arrangements seen at deeper levels give way to the first
544 appearance of looser arrangements, including parallel fibers (*Figure 8C,F*). Anti-5HT- and anti-
545 TH-immunoreactive fields are clearly segregated (*Figure 8A and D*) at or near the column origin
546 but begin to overlap at more rostral levels closer to the gyri, at locations where osmium-ethyl
547 gallate preparations show the columns branching, with tributaries extending to overlying gyri. At
548 those levels, immunoreactive processes appear to spread laterally into the gyri themselves
549 (*Figure 8G,H*).
550
551 **6. Organization of gyriform neuropils**
552 Five distinct gyri comprise the outer layer of the RLPR (*Figure 9A*). But only four gyri are
553 associated with the two calyces. A fifth proximal gyrus situated near the entry of the eyestalk
554 nerve is notable for its neuronal organization distinguishing it as entirely separate from the
555 mushroom body (*Figure 9A,F*).
556 Mass impregnations demonstrate at this outer level of the lateral protocerebum large
557 numbers of efferent neurons and their dendritic processes, many of which originate from clusters
558 of loosely arranged patches of perikarya that extend over the outer surface of the lateral
559 protocerebrum (*Figure 9 – figure supplement 1*). Although stochastically impregnated, the
560 abundance and variety of these neurons suggests the gyri contain dense arrangements of efferent
561 (output) and local interneurons (*Figure 9- figure supplement 1D-I*). Golgi impregnations reveal
562 swathes of axons extending across the gyri, suggesting lateral interactions amongst them.
563 Oblique palisades of dendritic trees, which have branching patterns peculiarly reminiscent of
564 vertebrate pyramidal cells (*Figure 9B*), send axons to fascicles that extend to the midbrain via
565 the eyestalk nerve.

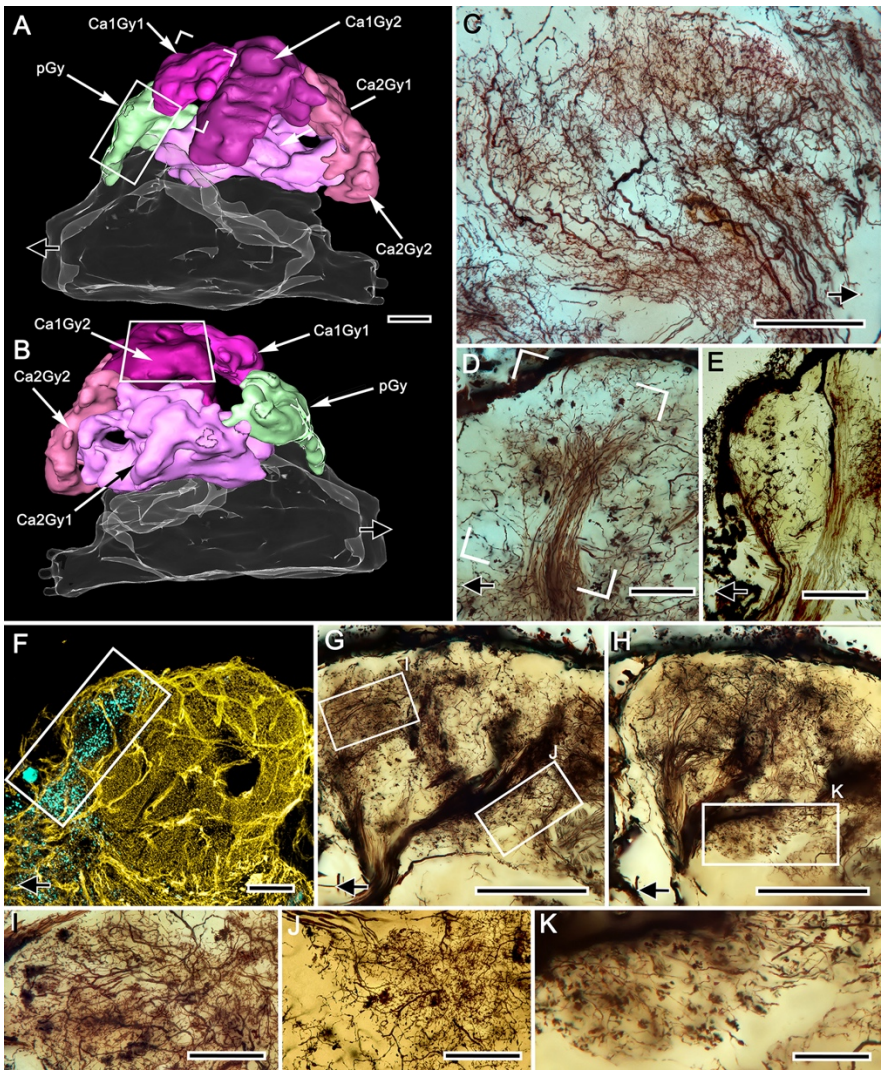

Figure 9. Gyriform neuropils: afferent and efferent organization. (**A, B**). Amira-generated 3–D reconstructions of the gyri and their calyces. Black arrows indicate the direction of the eyestalk nerve; likewise in panels C–H. (**C**) Ensemble of efferent dendrites in gyrus 2 associated with calyx 1 (Ca1Gy2). The represented area is boxed in panel B. (**D**) Afferent tributary from the antennoglomerular tract (olfactory projection neurons) suppling gyrus Ca1Gy1 neuropil (open rectangle in panel A). (**E**) Smooth oval presynaptic specializations denote the terminals of another antennoglomerular tributary that exclusively supplies the most proximal gyrus (pGY, rectangle in panel A), which has no obvious connection to the mushroom body. (**F**) Double-labelling with anti–GAD (yellow) and anti–allatostatin (cyan) of the lateral protocerebrum resolves allatostatin immunoreactivity in the proximal gyrus (rectangle in A and F), which shows little to no GAD immunoreactivity. (**G, H**) Stacked z-axis projections of Golgi-impregnated tracts, imaged through two successive 50-μm sections showing massive supply by afferent neurons. These reach levels of the lateral protocerebrum that include those at and well beneath the gyriform layer (box I, panel G), including levels of the calyces (box J in panel G and box K in panel H). Notably, many efferent neurons relaying information from gyri (panel H) send their downstream axons from the lateral protocerebrum into these tracts. (**I-K**) Enlargements from regions indicated in G, H, but at sample thicknesses of less than 20 μm to isolate details obscured in flattened optical sections . Scale bars, A–C, F–H, 100μm; D,E, 50μm; I–K, 50μm.

Figure 9 —— figure supplement 1. Perikaryal distributions and gyri neurons

586 Like deeper levels of the lateral protocerebrum, gyri comprising this superficial level of
587 the lateral protocecerum are supplied by terminals of afferent neurons, the axons of which radiate
588 out from the eyestalk nerve. Many of these terminals are identified as originating from discrete
589 fascicles that comprise the antennal globular tract, denoting not only their identity as axons of
590 projection neurons from the olfactory lobes but suggesting that different classes of projection
591 neurons comprise different fascicles (*Figure 9D,E*). The terminals of projection neurons are
592 denoted by their swollen boutons, the different morphologies of which are distinctive. For
593 example, terminals spreading out over the surface of gyrus 1, belonging to calyx 1, have rough
594 ball-shaped profiles that are distinct from larger smooth boutons from extremely slender axons
595 supplying the fifth proximal gyrus (pGy in *Figure 9A,B,E*). That gyrus's large allatostatin-
596 immunoreactive processes and the paucity, even absence, of GAD-immunoreactive networks
597 suggests its complete independence from the mushroom body's organization (*Figure 9F*). Nor,
598 as shown by osmium-ethyl gallate, is this gyrus associated with any of the calyces' outward
599 extensions.
600 In addition to axons extending from the eyestalk nerve providing afferents to superficial
601 levels in the gyri, all levels in the rostral protocerebrum receive an abundant supply of terminals,
602 including many penetrating to deep levels of the calyces (*Figure 9G-K*). Again, it is worth
603 bearing in mind when viewing the images in Figure 9G, H that Golgi impregnations likely reveal
604 not more than a few percent of the constituent neurons providing these already dense
605 arrangements of incoming fiber tracts.
606
607 **7. Transitions to gyri**
608 We have shown that four gyri overlie two large columns, each extending from one of the two
609 calyces, as do occasional smaller finger-like extensions. Osmium-ethyl gallate demonstrates that
610 the columns bifurcate close to the gyri (*Figure 1A, 2D,E*), a feature also resolved in serial
611 reduced-silver-stained sections (*Figure 7 - figure supplement 1A-H*). However, neither method
612 allows the identification of a clear inner margin of a gyrus or an obvious termination of the
613 column. Here we consider neural arrangements that denote the ambiguity of the interface
614 between the mushroom body's columns and their corresponding gyri .
615

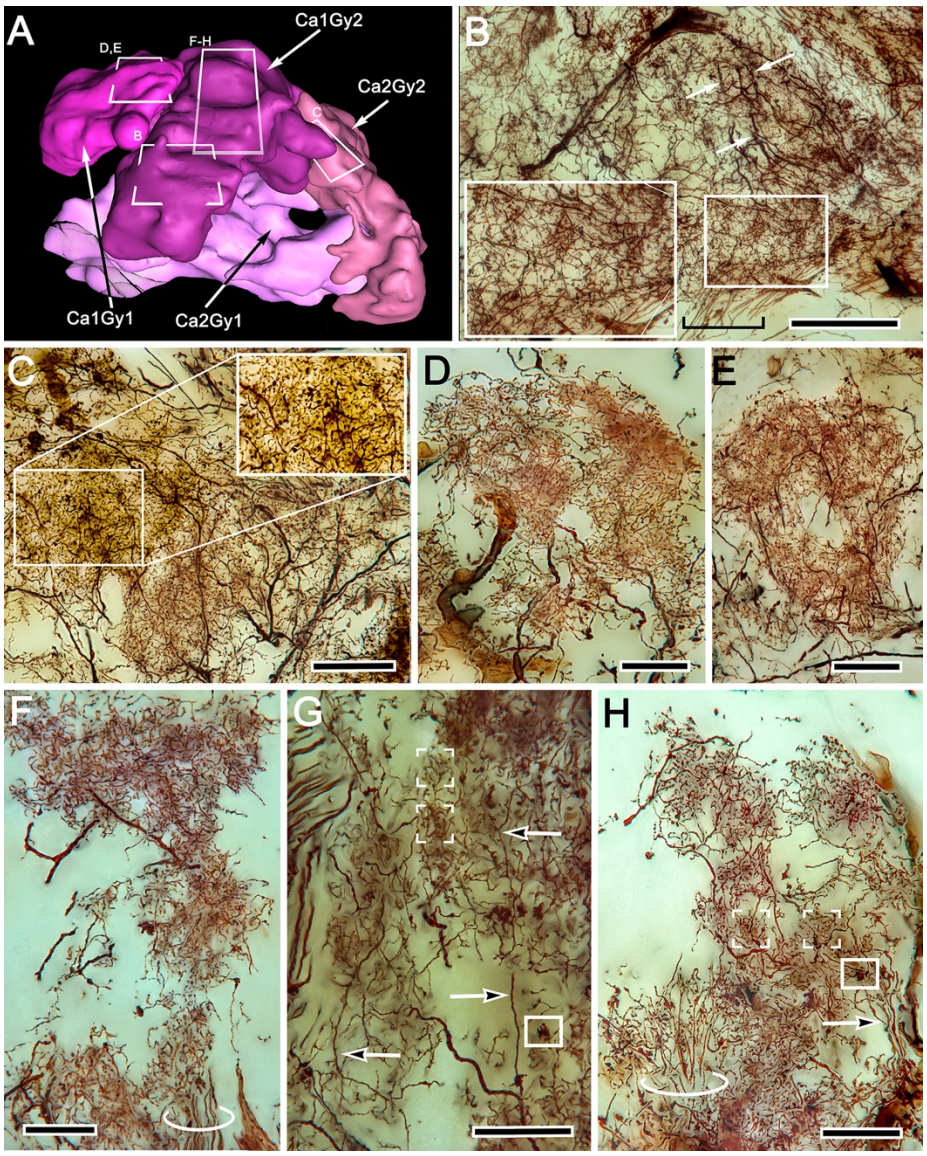

Figure 10. Gyrus neuropils: local circuit neurons. (**A**) 3-D reconstruction of gyri associated with calyx 1 and 2, showing approximate locations of networks shown in B–H. (**B**) Dense network supplied by ascending processes (boxed area is enlarged on left), ascribed to Ca1Gy2 derived from column 1. Dendrites of an efferent neuron (arrows) spread through this layer. (**C**) Efferent dendrites overlap a broad field of dense terminal specializations. Gnarled bouton-like specializations (boxed and enlarged on right) show that terminals from the eyestalk nerve enter this level. (**D-H**) Dense and elaborately branched elements interpreted as local interneurons (D, E) and intrinsic elements of the column (F-H). Ascending processes (circled in F,H and arrowed in G,H) are further evidence of local circuits. Dense groups of converging processes (box brackets in G,H) correspond in size to afferent boutons (boxed in G,H). Scale bars, B, C, 100μm: D-H, 50μm.

Figure 10 —— figure supplement 1. Column-gyrus interface organization**.**

Tangential sections across the gyri demonstrate novel and as yet puzzling aspects of their composition (*Figure 10A,B*). One is the presence of dendritic trees, as in Figure 10B, here

632 represented by a single impregnated neuron, the axon of which groups with others extending to
633 the lateral protocerebral root of the eyestalk nerve. The dendrites are seen overlapping with
634 elaborate networks of finely branching processes that terminate in small bead-like swellings
635 suggestive of presynaptic specializations. This network (*Figure 10B*) derives from extremely thin
636 processes that ascend into the gyrus from outward extensions of the calyx (bracketed in *Figure*
637 *10B*). Further examples (*Figure 10C*) show that the dendrites of a gyrus's efferent neurons
638 overlap other arrangements of putative ascending presynaptic fields. In this example, the fields
639 do not appear to be part of an intervening synaptic network but instead their disposition with the
640 efferent dendritic trees suggests that they likely terminate there (*Figure 9C*). In addition, highly
641 restricted systems of mixed spiny and beaded arborizations suggest local anaxonal neurons that
642 may provide synaptic interfaces between such terminal systems arising from the columns and the
643 dendrites of gyral efferent neurons (*Figure 10D,E*). Evidence that arborizations predominantly
644 equipped with presynaptic specializations likely originate from the calyces is indicated by
645 densely packed elements situated distally in the columns. These are equipped with short digiform
646 specializations arranged as small basket-like receptacles that clasp afferent terminals of unknown
647 origin (*Figure 10F-H*).
648 The rare Golgi impregnation that resolves one of the columns as a recognizable ensemble
649 of heterogeneous elements within the column's boundaries also demonstrates that its terminus is
650 "open," meaning contiguous with the gyral neuropil into which some of its fibers project (*Figure*
651 *7- figure supplement 1A; Figure 10 – figure supplement 1A*). Also fortuitous are preparations
652 that demonstrate the terminus of a column coinciding with bundled endings from the
653 antennoglomerular tract. Such a preparation (*Figure 10 supplement 1B*), also shows that the
654 terminus of the column is open to gyral neuropil around it and that processes extend from the
655 column into the gyrus. Combined labelling with anti-synapsin and actin at the terminus of the
656 column (*Figure 10 - figure supplement 1C*) further indicates that sizes and densities of sites
657 indicating synaptic convergence differ systematically across it. The flanking gyral neuropils also
658 betray substantial variation in synaptic densities. Inputs to the gyri do not, however, derive solely
659 from calycal columns and afferents from the antennoglomerular tract. Reduced silver shows that
660 tracts from caudal neuropil associated with the optic lobe extend rostrally to the superficial levels
661 of a gyrus (*Figure 10 - figure supplement 1D*), yet another indication of the complexity of
662 organization and its multimodal nature even at the most distal level of the mushroom body. The
663 possible significance of this is considered below in the Discussion.

664 **8. The reniform body**

665 We have shown that the lateral protocerebrum is divided into a rostral and caudal part (RLPR
666 and CLPR) , the former containing the paired mushroom bodies. The mushroom bodies are not,
667 however, the sole components of the RLPR. The pGy gyrus nearest to the RLPR's junction with
668 the eyestalk nerve is distinct and probably to some degree functionally separate from gyri
669 associated with the mushroom bodies (*Figure 9F*). In addition, there is another prominent system
670 of circumscribed neuropils situated close to the lateral border of the RLPR, arising from a dorsal
671 group of relatively small perikarya almost adjacent to the optic lobes. These neuropils comprise
672 the reniform body, a center identified in stomatopods by Bellonci (Bellonci, 1882), who
673 distinguished it from the very prominent mushroom bodies in that taxon. The same center has
674 been described in detail in the stomatopods *Neogonodactylus oerstedii*, *Gonodactylus smithii*,
675 and *G. chiragra*, and the carideans *Lebbeus groenlandicus* and *Alpheus bellulus.* In all these
676 species the reniform body adopts the same morphology: a densely populated bundle of axons,
677 referred to as the pedestal extends from the dorsal surface of the RLPR to its ventral surface,
678 providing four discrete neuropils called the initial (dorsal), lateral, and the ventrally situated
679 proximal and distal zones (Wolff et al., 2017; Thoen et al., 2019; Sayre and Strausfeld, 2019;
680 Strausfeld et al., 2020). In all of the cited taxa, the reniform body is situated between the
681 columnar mushroom body and the lobula.

682 Precisely the same placement is observed in the varunid lateral protocerebrum (*Figure*
683 *11*). The reniform body occupies a location lateral to the ensembles of neurons that constitute the
684 mushroom body gyri (*Figures 1,11*). Reconstructed from serial osmium-ethyl gallate sections,
685 the reniform body's pedestal lies immediately above, i.e., rostral to, the two tracts of neurites
686 from the globuli cell cluster (the globuli cell tract) that provide intrinsic neurons to the
687 mushroom body calyces (*Figure 11 C*). In *H. nudus*, the reniform body pedestal extends from a
688 mass of cell bodies at the dorsal surface and extends almost to the lateral protocerebrum's ventral
689 surface, bifurcating into two main tributaries about half way along its length (Figure 11 F). These
690 give rise to the lateral, distal and proximal zones, each zone composed of substantial volumes of
691 arborizations (*Figure 11 D*). The reniform body is thus entirely distinct from the mushroom
692 bodies, and is situated distally with respect to their centrally disposed calyces (*Figure 11 E*). The
693 reniform body's thick pedestal, albeit columnar in form, is distinct from a mushroom body
694 column in that its constituent axons are naked; lacking spines or other specializations that define
695 a mushroom body. The reniform body's four zones of branching collaterals contribute to

696 structures reminiscent of microglomeruli. However, they are of larger girth and synapsin-actin
697 labelling shows them to have significantly fewer converging presynaptic elements than a calycal
698 microglomerulus (*Figure 10, figure supplement 1D,E*). Despite these clear differences the
699 reniform body is strongly immunoreactive to anti-DC0 showing that it also is a learning and
700 memory center as demonstrated by Maza et al. (*Maza et al., 2016*).

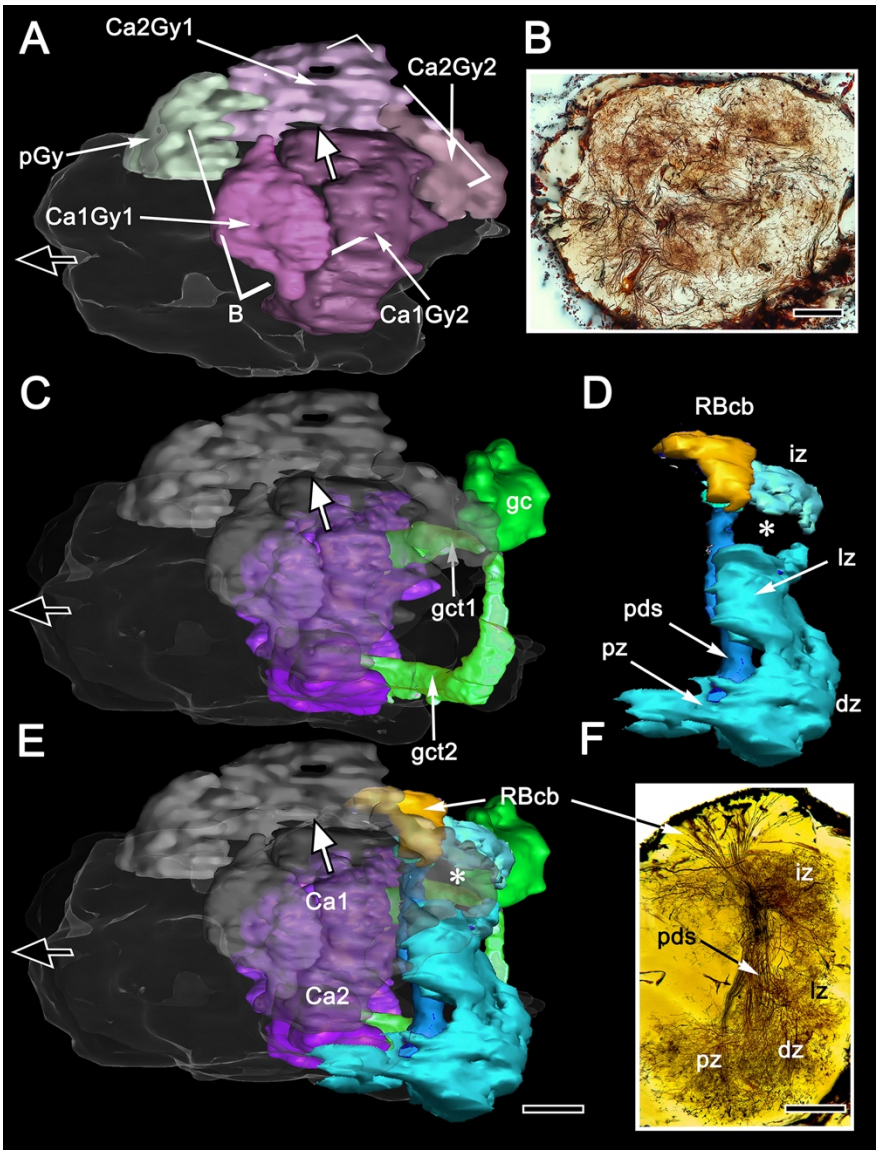

701

702 **Figure 11. Disposition of the reniform body.** (**A**) 3-D reconstruction of gyri from osmium-ethyl gallate
703 specimens identifies their 2:1 relationship with columns and their total volume, which can be compared to
704 the distribution of gyrus neurons resolved by Golgi impregnations (**B,** level indicated in A). The Golgi method
705 impregnates a fraction of the constituent neurons, the fields of which are mostly constrained to a gyrus.
706 Here impregnated neurons are viewed through the LPR's rostral surface. In panel A (and panels C E) the
707 black arrow indicates the medial axis, the white arrow the rostral axis. (**C**) The globuli cell cluster (gc)
708 provides two globuli cell tracts (gct1, gct2) to the two mushroom body calyces Ca1, Ca2. The lateral lobe
709 of gyrus 2 associated with calyx 2 (indicated by the asterisk in panel E) reaches out distally and fills a gap

710 (asterisk in D) between two processes (the intermediate and lateral zones, iz and lz) originating from the
711 reniform body's pedestal (pds). (**D**) The reniform body pedestal is a dense fiber bundle originating from a
712 dorsal cluster of small cell bodies (RBcb) on the distal flank of the RLPR. The pedestal's ventrally dividing
713 branches, shown Golgi-impregnated in panel **F**, provide the dorsal and proximal zones (dz, pz). (**E)**
714 Combined volumes in A,C, and D demonstrating the position and modest dimensions of the reniform body
715 relative to the mushroom bodies, comprising the calyces (Ca1, Ca2) and their columns and associated gyri.
716 Scale bars, A-C, B, F, 100μm.
717 **Figure 11 —— figure supplement 1**. Comparison of synaptic densities associated with the calyces and
718 reniform body.
719

720 ## Discussion

721 **Unique organization of the varunid mushroom body.** Studies by Hanström in the 1920s and
722 1930s on the brains of malacostracan crustaceans concluded that mushroom bodies equipped
723 with calyces and columns (lobes), as they are in insects and mantis shrimps (Bellonci, 1882),
724 have been reduced in decapods to columnless centers lying immediately beneath the rostral
725 surface of the lateral protocerebrum. Recent comparisons of the brains of reptantian decapods
726 have confirmed that its lineages share the evolutionary trend of reduction and loss of the
727 mushroom body column (Strausfeld and Sayre, 2019). Those mushroom bodies nevertheless
728 retain most elements of ancestral networks: diffusely arranged in Axiidea, Astacidea, Achelata
729 (Strausfeld and Sayre, 2019), but precisely stratified in terrestrial and marine Anomura, (hermit
730 crabs: Harzsch and Hansson, 2008; Wolff et al., 2012; Strausfeld and Sayre, 2019).
731 Ocypodidae (fiddler crabs) and Varunidae (shore crabs), two lineages of Brachyura (true
732 crabs) do not conform to this trend. As demonstrated previously and again here, large DC0-
733 positive domains cover much of the varunid lateral protocerebrum, suggesting relatively
734 enormous (for an arthropod) learning and memory neuropils (Strausfeld et al., 2020). The
735 proposition that the reniform body is the crab's mushroom body (Maza et al., 2016, 2020) is
736 refuted by Golgi impregnations and 3-D reconstructions of the lateral protocerebrum
737 demonstrating the reniform body as entirely distinct from the huge DC0-positive mushroom
738 body adjacent to it (*Figure 11*).
739 Similarity, conjunction, and congruence are established criteria for assessing phenotypic
740 homology (Patterson, 1988). In all the lineages where reniform bodies have been identified these
741 criteria exclude it as mushroom body homologue. That the brachyuran mushroom body has until
742 now remained unrecognized can be attributed to its hiding in plain sight as an unexpected and
743 radical reorganization. Even its population of conservatively estimated 20,000-30,000 densely
744 packed globuli cells is not where it would be expected to be based on other pancrustaceans.

745 Added to this difference is that the entire mushroom body is inverted such that its two
746 voluminous calyces are deeply buried in the rostral domain of the lateral protocerebrum where
747 they receive their inputs. These derive from the deutocerebrum's olfactory lobes and the
748 protocerebrum's optic lobes.
749 We show here that each calyx gives rise to a large column extending outwards and
750 merging with broad overlying gyri. The gyri are pillowed into folds and sulci thus forming a
751 cortex-like architecture. This system receives additional afferent supply and gives rise to
752 pyramidal-like ensembles of efferent neurons, the axons of which extend to the eyestalk nerve.
753 Throughout this massive structure, the mushroom body and its gyri are strongly immunoreactive
754 to antibodies raised against DC0.
755 Although the crab mushroom body appears vastly different from the right-way-up
756 "traditional" insect or stomatopod homologue, it nevertheless shares with them their defining
757 traits. For example, intrinsic neurons originating from globuli cells contribute to the brachyuran
758 calyces and columns as do the Kenyon cells of an insect mushroom body. As in stomatopods,
759 shrimps, and insects, the axon-like processes of intrinsic cells are clustered in their respective
760 fascicles, as they are in any one of the longitudinal divisions of the insect mushroom body
761 columns, where short intermingling collaterals can provide orthogonal connectivity (Strausfeld et
762 al. 2005; Sjöholm et al., 2005; Tanaka et al., 2008). Other longitudinal divisions of the varunid
763 mushroom body column are populated by intrinsic processes that interweave to provide
764 rectilinearity, as they do in one of the two mushroom body columns of the shrimp *Lebbeus*
765 *groenlandicus* (Sayre and Strausfeld, 2019), or in the stratified dome-like mushroom body of
766 hermit crabs (Wolff et al., 2015). We show here that true crabs express the whole panoply of
767 intrinsic cell arrangements. These include segregated and intermingling "parallel fibers" as in
768 Stomatopoda or the core lobe (column) of *Drosophila* (Wolff et al., 2017; Strausfeld et al.,
769 2003); rectilinear networks that extend part way into a column from the calyx; dense
770 arrangements of intrinsic processes extending across the columns comparable to certain neurons
771 populating the the mushroom body column in honey bees or crickets (Strausfeld 2002;
772 Hamanaka and Mizunami, 2019); and arrangements comparable to the longitudinal laminations
773 of the mushroom body lobes (columns) of Dictyoptera and Lepidoptera (Sinakevitch et al., 2001;
774 Sjöholm et al., 2005). In short, the crab mushroom body column appears to embody all known
775 arrangements across Pancrustacea. If each arrangement of a specific type of intrinsic neurons
776 represents a distinct computational property, as suggested from studies of honeybees and fruit

777 flies (Traniello et al., 2019; Perisse et al., 2016), then the crab would appear to be singularly
778 well-equipped. The same applies to its calycal arrangements, which in *H. nudus* are elaborate
779 and discretely partitioned into territories denoted by different morphologies of intrinsic neurons
780 and afferents. This zonal organization corresponds to the more compact and highly ordered
781 modality-specific domains typifying hymenopteran calyces (Gronenberg 2001), and, to a lesser
782 extent, *Drosophila* calyces as well (Yagi et al., 2016; Li et al., 2020).
783 The varunid lateral protocerebrum has two calyces, each providing a massive column.
784 This doubling of the calyx has many precedents. In the stomatopod lateral protocerebrum there
785 are four adjacent columns, each associated with a distinct ensemble of globuli cells and hence a
786 calyx. That organization has been compared to the *Drosophila* mushroom body, which is a
787 composite neuropil of four hemi-mushroom bodies derived from four clonal lineages, as it is in
788 the honey bee (Wolff et al., 2017; Ito et al., 1997; Farris et al., 2004). Consequently, the
789 mushroom bodies in an insect's lateral protocerebrum are paired but completely fused. The
790 varunid has two calyces in immediate contact, but not quite fused as no intrinsic neuron extends
791 its field of processes into both. Only one calyx (CA2) appears to receive input from a tract of
792 axons carrying relays from the medulla and from the reniform body. Such an asymmetric input to
793 twin calyces is not unique: a comparable arrangement is found in the *Drosophila* mushroom
794 body, where visual inputs terminate in an "accessary calyx" attached to one side of the fused
795 calyx (Vogt et al., 2016). A similar arrangement involving visual inputs has been described from
796 the swallowtail butterfly (Kinoshita et al., 2015).
797 Of particular note is the extensive organization of GAD-immunoreactive arborizations
798 that extend into every domain of the *H. nudus* calyces. These provide dense systems of minute
799 processes, the dispositions of which would allow synaptic contact with every neuronal process
800 supplying a microglomerus. Accepting that varunid intrinsic neurons correspond to insect
801 Kenyon cells, these GAD-immunoreactive systems suggest correspondence with wide-field
802 anaxonal inhibitory neurons that extend throughout the *Drosophila* calyx ('APL neurons': Liu
803 and Davis, 2009; Amin et al., 2020). Consequently, such putatively inhibitory anaxonal neurons
804 in the crab suggest a global role in local synaptic inhibition at microglomeruli. Arrangements of
805 aminergic neurons in the calyces and columns further correspond to mushroom body input and
806 output neurons recognized in *Drosophila* (Aso et al., 2014; Owald et al., 2015). It is also notable
807 that highly localized and densely branching TH- and 5HT- immunoreactive neurons occur at
808 different levels of the crab's calyces. These correspond to similar dispositions of immunoreactive

809 neurons in the layered calyces of columnar mushroom bodies, including those of stomatopods
810 and shrimps (Wolff et al., 2017; Sayre and Strausfeld, 2019). Neurons with the same
811 immunoreactive signatures are associated with columns, from their origin at the calyces out to
812 the level of their "fuzzy" interface with gyri and also in the gyri. Their successive levels in a
813 column approximate the arrangements of output neurons from successive partitions of insect
814 mushroom bodies, as exemplified in cockroaches and *Drosophila* (Li and Strausfeld, 1998;
815 Tanaka et al., 2008; Aso et al., 2014b); and in crustaceans by the successive fields of efferent
816 neurons in the mushroom bodies of Stomatopoda, Stenopodidea and Caridea (Wolff et al., 2017;
817 Sayre and Strausfeld, 2018; Strausfeld et al., 2020).
818
819 **Is the organization of gyri an outlier, and what is its homologue in other lineages?**
820 Comparisons of the varunid brain with those of other pancrustaceans meet an impasse when
821 considering the lateral protocerebrum's system of gyri, a cortex-like feature that appears to be
822 special to Brachyura. As described above, there is no obvious terminus of a mushroom body
823 column: its neurons merge with systems of local interneurons in the gyri and these local
824 interneurons extend amongst the dendrites of efferent neurons that leave the gyri. Might these
825 arrangements find corresponding organizations in other pancrustaceans and mandibulates? Or are
826 they exclusive to brachyuran crustaceans? And what developmental events might have given rise
827 to such a departure from the reptantian ground pattern?
828 With regard to the last question, two developmental studies on the reptantian lateral
829 protocerebrum should be noted, one on a brachyuran the other on an astacid. Both demonstrate
830 early stages of the formation of the larval lateral protocerebrum, in which there is not yet
831 evidence for morphogenetic reorganization in what will become the lateral protocerebrum
832 (Harzsch and Dawirs1996; Sintoni et al., 2007). However, as those authors indicated, crustaceans
833 undergo radical metamorphosis during the change from a pelagic larva to a preadult, the larval
834 stage providing pools of neural precursor cells for subsequent development. Those precursors
835 would likely contribute not only to the formation and differentiation of adult centers in the lateral
836 protocerebrum but also to any taxon-specific morphogenic rearrangements.
837 Might the relationship of the insect mushroom body MBONs to the rest of the brain
838 suggest an origin for the gyri? In insects, many of the mushroom body efferent neurons terminate
839 in neuropils of the superior medial protocerebrum (honeybee: Strausfeld, 2002; cockroach: Li
840 and Strausfeld 1997, 1999; *Drosophila*: Ito et al., 1998; Tanaka et al., 2008; Aso et al., 2014a,b).

841 This is the most rostral part of the forebrain in insects, comprising dense networks of local
842 interneurons that are interposed between the terminals of mushroom body outputs and the
843 dendrites of interneurons whose axons terminate in successive strata of the central complex's
844 fan-shaped body (Phillips-Portillo and Strausfeld, 2012). A comparable arrangement in
845 crustaceans with eyestalks requires that efferent neurons from the mushroom bodies extend their
846 axons into the midbrain's superior protocerebrum from a distant mushroom body situated in the
847 lateral protocerebrum. The likelihood of this connection is shown by silver-stained brains of *H.*
848 *grapsus* revealing numerous axons from the eyestalk nerve targeting the medial protocerebrum.
849 This would speak against gyri being medial neuropils displaced distally.
850 One possible interpretation of the gyri is that they represent enormously expanded
851 versions of tubercles, swollen parts of a column typifying mushroom bodies of certain caridid
852 shrimps (in Stenopodidae and Thoridae: Sayre and Strausfeld 2019) and insects (Zygentoma,
853 Ephemeroptera: Farris, 2005). Tubercles of caridid (or insect) mushroom bodies are compact,
854 comprising tangled extensions of intrinsic neuron processes associated with a concentrated
855 system of TH- and 5HT-immunorecative processes intersecting that level of the column. Those
856 arrangements are absent from gyri. Although there are TH- and 5HT-immunorecative fields in
857 gyri, these do not appear to interact with intrinsic fibers in the columns. Nevertheless, that gyri
858 are as strongly DC0-immunoreactive as the calyces and columns suggests that they play crucial
859 roles in memory acquisition.
860 Far more elaborated than a tubercle, gyri comprise many morphologically distinct types
861 of neurons, including efferents of unknown antigenicity. The presence in gyri of local
862 interneurons and rectilinear networks further indicates an identity that is indirectly associated
863 with the mushroom body. A clue is suggested by other Reptantia, in which certain mushroom
864 body outputs target neuropils at deep levels of the lateral protocerebrum (Mellon et al., 1992a,b;
865 McKinzie et al., 2003). If these less well-studied neuropils became inverted, they would overlie
866 the inverted brachyuran mushroom bodies as do the gyri. In that scenario, the relationship
867 between a mushroom body and its target neuropils is essentially the same as in other reptantians,
868 except a consequence of inversion is that those neuropils have been able to undergo unparalleled
869 lateral expansion and gyrification.
870 **Correspondence with hippocampal evolution and function**
871 The entire ensemble, the inverted mushroom body and its associated gyri, has a fascinating
872 parallel in vertebrates (Figure 12). In vertebrates, the hippocampus originated as a planar

structure contiguous with a three-layered lissencephalic pallium; an arrangement typifying agnathans (Suryanarayana et al., 2017) and maintained across all vertebrate lineages other than mammals (Vargas et al., 2000; Striedter, 2016; Bingman and Muzio, 2017). In mammals, both the hippocampus and the pallium have undergone a defining modification: the hippocampus has become buried beneath the cerebral cortex, which concomitantly gained additional computational layers, gyrification and expansion (Ashwell and Gurovich, 2019). Those changes, historically proposed from comparative neuroanatomy (Hevner, 2016; Bingman and Muzio, 2017) have been firmly established by transcriptomics showing homology of the planar reptilian hippocampus with its sub-cortical counterpart in mammals (Tosches et al., 2018).

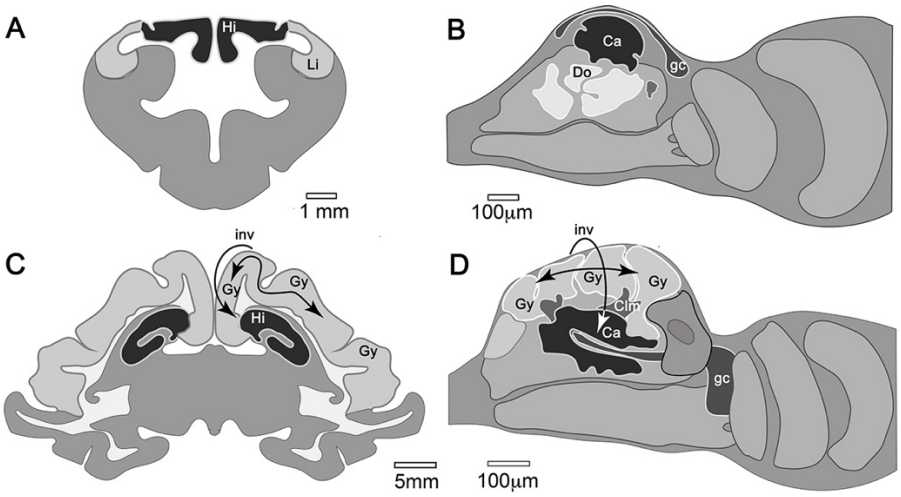

Figure 12. Convergent evolution of hippocampal and mushroom body inversion, burial, and gyriform expansion of target neuropils. (**A**) The turtle *Trachemys scripta elegans* illustrates the disposition of the reptilian hippocampus (Hi) as continuous with a three layered lissencephalic cortex (Li). (**B**) The crustacean equivalent of this organization is exemplified by the crayfish *Procambarus clarkia,* where the lobeless mushroom body (Ca) lies at the rostral surface of the brain above domains receiving the mushroom body's output neurons (Do). (**C**) The monotreme *Tachyglossus aculeatus* exemplifies the disposition of the hippocampus (Hi) in mammals, where its inverted: folded neuropils are buried beneath a gyriform cortex (Gy). (**D**) The crustacean equivalent is represented by the varunid crab *Hemigrapsus nudus* in which the inverted mushroom body calyx (Ca) is buried beneath the rostrally arranged gyriform neuropils (Gy). Gc, globuli cells. Scale bars: A, 1 mm; B, 100 μm; C, 5mm; D, 100 μm.

In reptantian crustaceans columnless mushroom bodies located at the brain's outer surface approach a disposition seen in non-mammalian vertebrates. But in Brachyura, evidence described here indicates its rostral lateral protocerebrum has become inverted. Both the subcortical burial of the hippocampus in mammals and an inverted mushroom body in brachyurans allow room for the expansion of neuropils to which they communicate, in mammals the six layered cortex, in varunid brachyurans the gyri, thus supporting the evolution of novel

900 circuitry for memory acquisition and cognitive attributes enabling competition and territorial
901 dominance through the awareness of place.
902
903 **Is genealogical correspondence of the hippocampus and panarthropod mushroom body**
904 **plausible?** It has been argued that the vertebrate cerebellum would be the most fitting
905 homologue of the insect mushroom body because both centers are defined by comparable
906 arrangements of parallel fibers (Schürmann, 1987; Farris, 2011, Li et al., 2020). Despite there
907 being no organization in any mushroom body that is as strictly parallel as in the cerebellum, the
908 strongest argument against this proposition is that the mushroom body arises rostral to the brain's
909 deutocerebral-tritocerebral boundary, which is the homologue of the vertebrate midbrain-
910 hindbrain boundary, in front of which the hippocampus and pallium also originate (Bridi et al.,
911 2020).
912 Several lines of evidence suggest that the hippocampus and mushroom bodies may
913 correspond genealogically. Shared traits include detailed neuroanatomical conformities, intense
914 immunoreactivity to antibodies raised against DC0 (Strausfeld, 2012; Wolff and Strausfeld,
915 2015), and in *Drosophila* orthologues of at least 15 genes relating to neuronal specification and
916 cognitive functions in the rodent hippocampus (Wolff and Strausfeld, 2015). Homologous gene
917 expression has been shown during development of the *Drosophila* mushroom body, the murine
918 pallium, and the mushroom body of the polychaete *Platynereis* (Tomer et al., 2010). Neuronal
919 arrangements of intrinsic and extrinsic neurons in the mushroom bodies of polychaete annelids
920 correspond to those of insect mushroom bodies (Strausfeld et al., 1998; Wolff and Strausfeld,
921 2015; Heuer and Loesel, 2009). This, and their DC0-immunoreactivity (Wolff and Strausfeld,
922 2015) could further suggest that mushroom bodies originated before the divergence of
923 protostomes and deuterostomes.
924 The present account adds another line of evidence for correspondence of the
925 hippocampus and pancrustacean mushroom body. Mushroom bodies also mediate functional
926 roles comparable to those mediated by hippocampi, the most tantalizing being the canonical
927 ability of many species to recall numerous locations during navigation and exploration (Krebs et
928 al., 1989; Day et al., 2001; López et al, 2003; Salas et al., 2003). Lesions of the hippocampus
929 impair place memory, as do lesions of mushroom body columns (Clark et al., 2005; Mizunami et
930 al., 1998), a deficit confirmed by reversible chemical silencing of the homologous network in
931 ants (Buehlmann et al., 2020; Kamhi et al., 2020). Comparisons of species adept at broad

932 exploration versus those with constrained ranges demonstrate that spatial exploration relates to
933 enlarged mushroom bodies, another property shown for the vertebrate hippocampus
934 (Montgomery et al., 2016; van Djik et al., 2017). These disparate yet intersecting lines of
935 evidence suggest that particularly voluminous mushroom bodies indicate a species' reliance on
936 spatial or social cues, as is true for the mammalian or avian hippocampus (Withers et al., 1993,
937 2008; Ott and Rogers, 2010; Molina and O'Donnell, 2007, 2008; Healy and Krebs, 1992). That
938 brachyuran species demonstrate comparable abilities (Jacoby, 1981; Tanner and Jackson, 2012;
939 Davies et al., 2019) is not surprising in the light of the present findings.
940

941 **Materials and Methods**

942

943 **Animals.** Crabs (*Hemigrapsus nudus*), with carapace widths between 6 and 8 cms, were
944 collected from designated sites on San Juan Island, Washington, affiliated with the Friday
945 Harbor Marine Biology Laboratory (University of Washington, Seattle). Two further shipments
946 of living crabs were sent to the Strausfeld laboratory and maintained at 15˚C in tanks containing
947 seaweed continuously moistened with salt water. A total of 76 animals were used for this study
948 over an 8-year period. Twenty were used for immunohistology, 8 for osmium-ethyl gallate
949 staining, 10 for Bodian reduce silver staining and 38 for Golgi impregnations.
950

951 **Neuropil staining with osmium-ethyl gallate**. A modified ethyl gallate method (Wigglesworth
952 1957) was used to stain entire brains that were then embedded in plastic and serial sectioned.
953 These were used for Amira 3D reconstructions. After cooling to complete immobility, the
954 eyestalks were opened to expose the lateral protocerebrum. The head was then immediately
955 sliced off behind the brain and with the eyestalks immersed in 0.13 M cacodylate buffered (pH
956 6.8; Fisher Scientific, Cat#: 50-980-232) 1% paraformaldehyde with 2% glutaraldehyde
957 (Electron Microscopy Sciences, Hatfield, PA). The rest of the animal was placed in a -40˚C
958 freezer. After overnight fixation undissected tissue was soaked in buffer. The lateral protocebra
959 and midbrain were then freed of overlying exoskeleton. Next, tissue was placed for 2 h in 0.5%
960 osmium tetroxide in cacodylate buffer, continuously rocked and kept at around 4˚C in the dark.
961 After a washing in cold buffer, tissue was further well washed in distilled water while raising the
962 temperature to 20˚C. Tissue was then immersed in aqueous 0.5% ethyl gallate with constant

963 rocking. Tissue was periodically checked and when dark blue (after about 30 minutes)
964 thoroughly washed in distilled water, dehydrated, and embedded in Durcupan to be cut serially
965 into 15µm thick serial sections using a sliding microtome.
966
967 **Neuropil staining with reduced silver**. Bodian's original method (Bodian, 1936) was used, after
968 fixing tissue in an admixture consisting of 75 parts absolute ethanol, 5 parts glacial acetic acid,
969 20 parts 16% paraformaldehyde (Electron Microscopy Sciences; Cat# 16220; Hatfield, PA). As
970 for the osmium-ethyl gallate method, crabs were cooled to complete immobility, the relevant
971 parts removed, opened and fixed in AAF (70 parts absolute ethanol, 5 parts glacial acetic acid,
972 25 parts 10% E. M. grade formaldehyde). After 2-4 hours neural tissue was freed under 70%
973 ethanol, then dehydrated to absolute ethanol before clearing in terpineol. It was next soaked in
974 Xylol raising the temperature to 65˚C. Finally, tissue was transferred, via a mixture of 50:50
975 Xylol-Paraplast, into pure Paraplast (Sherwood Medical, St. Louis, MO) held at 65˚C in shallow
976 aluminum cookie dishes. After three changes, each about 3-4 minutes long, the final dish was
977 placed on icy water for the Paraplast to immediately begin to solidify. After serial sectioning at
978 10µm, sections were mounted on glycerin-albumin-subbed slides, dried, and dewaxed. Hydrated
979 material was incubated at 60˚C in 2-5% silver proteinate (Roques, Paris) for 24 h with the
980 addition of 1-4 g pure copper shot/100 ml. Afterward, sections were conventionally treated with
981 hydroquinone, gold toned, fixed, and mounted under Permount (Fisher, Springfield, NJ).
982
983 **Silver chromate (Golgi) impregnation**. Animals were anesthetized over ice. The midbrain and
984 eyestalk neural tissue was dissected free from the exoskeleton and its enveloping sheath in ice-
985 cold chromating solution comprising 1 part 25% glutaraldehyde (Electron Microscopy Sciences;
986 Cat# 16220; Hatfield, PA), 5 parts 2.5% potassium dichromate (Sigma Aldrich; Cat# 207802; St.
987 Louis, MO) with 3–12% sucrose, all dissolved in high pressure liquid chromatography (HPLC)-
988 grade distilled water (Sigma Aldrich; Ca#270733). Central brains and their detached lateral
989 protocerebra (tissues) were placed in fresh chromating solution overnight, in the dark at room
990 temperature (RT). Next, tissues were briefly rinsed (30 seconds with swirling) in 2.5% potassium
991 dichromate and transferred to an admixture of 2.5% potassium dichromate and 0.01% osmium
992 tetroxide (Electron Microscopy Sciences; Cat# 19150; Hatfield, PA) for 24 hrs. Tissues were
993 again washed in 2.5% potassium dichromate and immersed for 24 hr. in a fresh chromating

994 solution. Before silver impregnation, tissues were decanted into a polystyrene weighing dish,
995 swirled in 2.5% potassium dichromate and then gently pushed with a wooden toothpick into a
996 glass container containing fresh 0.75% silver nitrate (Electron Microscopy Sciences; Cat# 21050;
997 Hatfield, PA) in HPLC water. Tissues were twice transferred to fresh silver nitrate, then left
998 overnight in silver nitrate. Throughout, metal was not allowed to come into contact with tissue.
999 Tissues were rinsed twice in HPLC water. To achieve massive impregnation of neurons, after
1000 treatment with silver nitrate tissues were washed in HPLC water and again immersed in the
1001 osmium-dichromate solution for 12hrs. and then transferred to silver nitrate as described above.
1002 After washing in HPLC water and dehydration through a four step ethanol series from 50% to
1003 100% ethanol tissues were immersed in propylene oxide (Electron Microscopy Sciences; Cat#
1004 20401; Hatfield, PA), and left for 15min. They were then subject to increasing concentrations of
1005 Durcupan embedding medium (Sigma Aldrich; Cat# 44610; St. Louis, MO) in propylene oxide
1006 during 3-5 hours. Tissues were left overnight at RT in pure liquid Durcupan and then
1007 individually oriented in the caps of BEEM capsules. These were then married to the inverted
1008 capsule cut open at its base, and were topped–up with Durcupan. Filled capsules were placed in a
1009 60°C oven for 18–24 hr. for plastic polymerization. Cooled blocks were sectioned at a thickness
1010 of 40-50µm (max) and mounted using Permount mounting medium (Fisher Scientific; Cat#
1011 SP15-100; Hampton, NH).
1012
1013 **Immunohistochemistry, antibodies**. Visualization of arrangements of immunostained neurons
1014 that further define mushroom bodies was achieved using antibodies listed in Table 1. An
1015 antibody against DC0 that recognizes the catalytic subunit of protein kinase A in D.
1016 melanogaster (Skoulakis et al., 1993) is preferentially expressed in the columnar lobes of
1017 mushroom bodies across invertebrate phyla, including members of Lophotrochozoa (Wolff &
1018 Strausfeld, 2015). Western blot assays of DC0 antibodies used on cockroach, crab, centipede,
1019 scorpion, locust, remipede, and millipede neural tissue reveal a band around 40 kDa, indicating
1020 cross-phyletic specificity of this antibody (Stemme et al., 2016; Wolff & Strausfeld, 2015).
1021 Antibodies against synapsin (Klagges et al., 1996) and α-tubulin (Thazhath et al., 2002) were
1022 used, often in conjunction with other primary antibodies, to identify dense synaptic regions and
1023 general cellular connectivity. Both antibodies likely recognize highly conserved epitope sites
1024 across Arthropoda and have been used previously in crustaceans (Andrew et al., 2012; Brauchle
1025 et al., 2009; Harzsch et al., 1997; Harzsch & Hansson, 2008; Sullivan et al.,, 2007). Antibodies

1026 against serotonin (5HT), glutamic acid decarboxylase (GAD), and tyrosine hydroxylase (TH)
1027 were used in this study to describe neuronal organization and in distinguishing neuropil
1028 boundaries. 5HT is an antibody that has proven to be invaluable for neuroanatomical studies
1029 across Arthropoda (Antonsen & Paul, 2001; Harzsch & Hansson, 2008; Nässel, 1988). Previous
1030 studies have used 5HT as a comparative tool for neurophylogenetic analysis (Harzsch &
1031 Waloszeck, 2000). Antibodies against GAD and TH were used to detect the enzymatic
1032 precursors of gamma aminobutyric acid (GABA) and dopamine, respectively. These two
1033 antibodies do not require the use of alternative fixation methods, making them compatible with
1034 synapsin and α-tubulin labeling, while avoiding the need to use glutaraldehyde. Comparisons of
1035 anti-GAD and anti-TH immunolabeling with that of their respective derivatives have
1036 demonstrated that these antibodies, respectively, label putative GABAergic and dopaminergic
1037 neurons (Cournil et al, 1994; Crisp et al., 2001; Stemme et al., 2016; Stern, 2009).
1038
1039 **Immunohistochemistry, application:** Methods follow those used for two recent studies on the
1040 eumalacostracan brain (Sayre & Strausfeld, 2019; Strausfeld et al., 2020). Animals were
1041 anesthetized to immobility using ice. Brains detached from nerve bundles leading to the
1042 eyestalks were first dissected free and the eyestalks were then removed. Immediately after
1043 removal, tissue was immersed in ice-cold fixative (4% paraformaldehyde in 0.1 M phosphate-
1044 buffered saline (PBS) with 3% sucrose [pH 7.4]). Midbrains and lateral protocerebra with their
1045 intact optic lobes were desheathed and left to fix overnight at 4˚C. Next, tissue was rinsed twice
1046 in PBS before being transferred to the embedding medium (5% agarose with 7% gelatin) for 1
1047 hr. at 60˚C before cooling to room temperature in plastic molds. After solidification, blocks were
1048 removed from the molds and postfixed in 4% paraformaldehyde in PBS for 1 hr. at 4˚C. The
1049 blocks were then rinsed twice in PBS and sectioned at 60 µm using a vibratome (Leica VT1000
1050 S; Leica Biosystems, Nussloch, Germany). Next, tissue sections were washed twice over a 20
1051 min. period in PBS containing 0.5% Triton-X (PBST). Tissue was subsequently blocked in
1052 PBST with 0.5% normal donkey serum (NDS; Jackson ImmunoResearch; RRID:AB_2337258)
1053 for 1hr before primary antibody incubation. Primary antibodies were added to the tissue sections
1054 at dilutions listed in Table 1. Sections were left overnight on a rotator at room temperature.
1055 Sections were next rinsed in PBST six times over the course of an hour. Donkey anti-mouse Cy3
1056 and donkey anti-rabbit Cy5 or Alexa 647 (Jackson ImmunoResearch; RRID: AB_2340813;

1057 RRID: AB_2340607; RRID: AB_2492288, respectively) IgG secondary antibodies were added
1058 to Eppendorf tubes at a concentration of 1:400 and spun for 12 min at 11,000 g. The top 900 µL
1059 of the secondary antibody solution was added to the tissue sections, which were then left to
1060 incubate overnight at room temperature on a rotator. For F-actin staining, tissue sections were
1061 left to incubate in a solution containing phalloidin conjugated to Alexa 488 (Thermo Fisher
1062 Scientific; RRID: AB_2315147) at a concentration of 1:40 in PBST for 2–3 days with constant
1063 gentle agitation following secondary antibody incubation. To label cell bodies, tissue sections
1064 were then rinsed twice in 0.1 M Tris–HCl buffer (pH 7.4) and soaked for 1 hr. in Tris–HCl
1065 buffer containing 1:2000 of the nuclear stain, Syto13 (ThermoFisher Scientific; Cat# S7575) on a
1066 rotator. Next, sections were rinsed six times in Tris–HCl over the course of 1 hr. before being
1067 mounted on slides in a medium containing 25% Mowiol (Sigma Aldrich; Cat# 81381) and 25%
1068 glycerol in PBS. Slides were covered using #1.5 coverslips (Fisher Scientific; Cat# 12-544E). To
1069 verify secondary antibody specificity, primary antibodies were omitted resulting in complete
1070 abolishment of immunolabeling. TH immunolabeling required a modified staining procedure
1071 with a shorter fixation time as well as antibody incubation in whole unsectioned tissue. Standard
1072 fixation times or sectioning the tissue prior to immunostaining resulted in poor or absent labeling
1073 as has been described previously (Cournil et al., 1994; Lange & Chan, 2008). For TH labeling,
1074 neural tissue was dissected and fixed in 4% paraformaldehyde in PBS containing 3% sucrose for
1075 30–45 min. Following fixation, neural tissue was rinsed twice in PBS, and then twice in 0.5%
1076 PBST over the course of 40 min. Tissue was then transferred to blocking buffer containing 5%
1077 NDS in 1% PBST and left to soak for 3 hr. TH primary antibody was next added to the blocking
1078 buffer at a concentration of 1:250. To assist antibody permeation, whole tissues were
1079 microwave-treated for 2 cycles of 2 min on low power (~80 W) followed by 2 min no power
1080 under a constant vacuum. Tissue was subsequently left to incubate in primary antibody solution
1081 for 2–3 days and was microwave-treated each day. After primary antibody incubation, tissue was
1082 washed with 0.5% PBST six times over the course of 2 hr. and then transferred to a solution
1083 containing 1:250 Cy3 secondary antibody. Whole mounts were left in secondary antibody
1084 overnight on a gentle shaker before being sectioned and mounted as described above. In dual
1085 labeling experiments, sectioned tissue labeled with anti-TH was then stained with an additional
1086 primary and secondary antibody also as described above.
1087

1088 **Imaging**. Confocal images were collected as Tiff files using a Zeiss Pascal 5 confocal
1089 microscope (Zeiss; Oberkochen, Germany). Image projections were made using Zeiss Zen
1090 System software. Light microscopy images were obtained using a Leitz Orthoplan microscope
1091 equipped with Plan Apochromat oil-immersion objectives (X40, X60, and X100). Series of step-
1092 focused optical sections (0.5–1.0 µm increments) were collapsed onto a single plane using
1093 Helicon Focus (Helicon Soft; Kharkov, Ukraine). Images were transferred to Adobe Photoshop
1094 (Adobe Systems, Inc; San Jose, CA) and processed using the Photoshop camera raw filter plug-
1095 in to adjust sharpness, color saturation and luminance, texture and clarity.
1096
1097 **3D-reconstruction**
1098
1099 Serial sections of osmium-ethyl gallate stained eyestalks were imaged using a brightfield Leitz
1100 Orthoplan microscope at a pixel scale of 0.5 µm x 0.5 µm. The sections were cut at a thickness
1101 of 15 µm using a rotating microtome. To account for compression and error using dry lenses
1102 because of the difference in refractive indices between glass/section and air, image sections were
1103 digitally adjusted to a voxel size of 0.5 µm x 0.5 µm x 24 µm. Additionally, to obtain a better Z-
1104 resolution, two snapshots at two focus planes were taken for each section. The resulting images
1105 were manually aligned using non-neuronal fiduciaries in the software TrakEM2 (Cardona et al.,
1106 2012).
1107 Neuropils, cell bodies, and large nerve tracts were segmented using the software Amira
1108 (Amira 2019.4; Thermo Fisher Scientific; Waltham, MA; USA). We achieved this using the
1109 Segmentation Editor, a tool which enables tracing of image data by assigning voxels to materials
1110 (i.e. user defined objects such as neuropils, cell bodies, etc.) using a paintbrush tool. Selected
1111 sections were outlined in the XY plane and interpolated across sections. Then, using the aid of
1112 the interpolated outlines, selected sections were traced in the XY, YZ and XZ planes to create a
1113 scaffold of the region of interest. The function "wrap" was then used to interpolate a 3D
1114 reconstruction of the object constrained by the scaffold. For visualization purposes, the label
1115 field containing "wrapped" labels was interpolated in Z using the "Interpolate Labels" module,
1116 adding an additional three slices for each already existing slice while maintaining the overall
1117 dimension of the reconstruction. This helped to account for the anisotropic Z-resolution (i.e.
1118 "staircase effect"). The 3D model was then visualized using the "Surface Generator" module,
1119 which created a 3D polygonal surface mesh. Images used for the figures were generated using

1120 the snapshot function. The globuli cell population was estimated on the basis of spherical

1121 globuli cells, each with the average radius of 3μm, occupying a volume of

1122 $2.5074^3 \mu m^3$ calculated from the serially reconstructed globuli cell mass.

1123

1124

Key Resources Table				
Reagent type (species) or resource	**Designation**	**Source or reference**	**Identifiers**	**Additional information**
Biological sample	*Hemigrapsus nudus*	Friday Harbor Laboratories	N/A	n=76
Antibody	α-Tubulin (Mouse, monoclonal)	Developmental Studies Hybridoma Bank (DHSB)	CAT#: 12G10; RRID: AB_1157911	1:100
Antibody	α-Tubulin (Rabbit, polyclonal)	Abcam	CAT#: ab15246; RRID: AB_301787	1:250
Antibody	Synapsin (SYNORF1; Mouse, monoclonal)	Developmental Studies Hybridoma Bank (DHSB)	CAT#: 3C11; RRID: AB_528479	1:100
Antibody	Serotonin (5HT; Rabbit, polyclonal)	ImmunoStar	CAT#: 20080; RRID: AB_572263	1:1000
Antibody	Glutamic acid decarboxylase (GAD; Rabbit, polyclonal)	Sigma-Aldrich	CAT#: G5163; RRID: AB_477019	1:500
Antibody	Tyrosine hydroxylase (TH; Mouse, monoclonal)	ImmunoStar	CAT#: 22941; RRID: AB_572268	1:250
Antibody	Allatostatin (Ast7; Mouse, monoclonal)	Developmental Studies Hybridoma Bank (DHSB)	CAT#: 5F10; RRID:AB_528076	1:100
Antibody	DC0 (Rabbit, polyclonal)	Generous gift from Dr. Daniel Kalderon (Skoulakis et al., 1993)	RRID: AB_2314293	1:400
Antibody	AffiniPure Donkey Anti-Mouse IgG (H+L) Cy™3 (polyclonal)	Jackson ImmunoResearch	CAT#: 715-165-150; RRID: AB_2340813	1:400
Antibody	AffiniPure Donkey Anti-Rabbit IgG (H+L) Cy™5 (polyclonal)	Jackson ImmunoResearch	CAT#: 711-175-152; RRID: AB_2340607	1:400

Antibody	AffiniPure Donkey Anti-Rabbit IgG (H+L) Alexa Flour® 647 (polyclonal)	Jackson ImmunoResearch	CAT#: 711-605-152; RRID: AB_2492288	1:400
Other (serum)	Normal donkey serum	Jackson ImmunoResearch	RRID: AB_2337258	N/A
Other (DNA stain)	SYTO™ 13 Green Fluorescent Nucleic Acid Stain	Thermo Fisher Scientific	CAT#: S7575	1:2000
Other (Phalloidin stain)	Alexa Fluor™ 488 Phalloidin	Thermo Fisher Scientific	CAT#: 12379; RRID: AB_2315147	1:40
Other (Chemical)	α-terpineol	Sigma-Aldrich	CAT#: 432628	N/A
Other (histology chemical)	Potassium dichromate	Sigma-Aldrich	CAT#: 207802	N/A
Other (HPLC purified water)	HPLC WATER	Sigma-Aldrich	CAT#: 270733	N/A
Other (histology chemical)	Osmium tetroxide	Electron Microscopy Sciences	CAT#: 19150	N/A
Other (histology chemical)	Ethyl gallate	Fisher Scientific	CAT#: G001625G	N/A
Other (histology chemical)	Phosphate buffer tablets	Sigma-Aldrich	CAT#:45ZE83	N/A
Other (histology chemical)	Glutaraldehyde	Electron Microscopy Sciences	CAT#: 16220	N/A
Other (histology chemical)	Paraformaldehyde	Electron Microscopy Sciences	CAT#: 15710	N/A
Other (histology chemical)	Sodium cacodylate	Electron Microscopy Sciences	CAT#: 50-980-232	N/A
Other (histology chemical)	Silver nitrate	Electron Microscopy Sciences	CAT#: 21050	N/A
Other (histology chemical)	Pure copper shot	Sigma-Aldrich	CAT#: 326488	N/A
Other (histology chemical)	Propylene oxide	Electron Microscopy Sciences	CAT#: 20401	N/A
Other (embedding resin)	Durcupan™ ACM resin (4-part component kit)	Sigma-Aldrich	CAT#: 44610	N/A
Other (embedding medium)	Paraplast Plus	Sigma-Aldrich	CA#: 76258	N/A
Other (mounting medium)	Permount mounting medium	Fisher Scientific	CAT#: SP15-100	N/A
Other (mounting medium)	Entellan	Sigma-Aldrich	CAT#: 1.07961	N/A

Software, algorithm	Photoshop CC	Adobe Inc.	N/A	N/A
Software, algorithm	Helicon Focus	Helicon Soft	N/A	N/A
Software, algorithm	Zen System Software	Zeiss	N/A	N/A
Software, algorithm	TrakEM2	Cardona et al., 2012	N/A	N/A
Software, algorithm	Amira 2019.4	Thermo Fisher	N/A	N/A
Other (microscope)	LSM 5 Pascal confocal microscope	Zeiss	N/A	N/A
Other (microscope)	Orthoplan light microscope	Leitz	N/A	N/A

References

Amin H, Apostolopoulou AA, Suárez-Grimalt R, Vrontou E, Lin AC. 2020. Localized inhibition in the Drosophila mushroom body. *eLife 2020*. **9**:e56954 DOI: 10.7554/eLife.56954

Andrew DR, Brown SM, Strausfeld NJ. 2012 The minute brain of the copepod *Tigriopus californicus* supports a complex ancestral ground pattern of the tetraconate cerebral nervous systems. *Journal of Comparative Neurology* **520**:3446–3470. https://doi.org/10.1002/ cne.23099

Antonsen BL, Paul DH. 2001. Serotonergic and octopaminergic systems in the squat lobster *Munida quadrispina* (Anomura, Galatheidae). *Journal of Comparative Neurology* **439**:450–468. https://doi.org/10.1002/cne.1362

Ashwell KWS, Gurovich Y. 2019. Quantitative analysis of forebrain pallial morphology in monotremes and comparison with that in therians. *Zoology* **134**:38-57. https://doi.org/10.1016/j.zool.2019.04.002.

Aso Y, Hattori D, Yu Y, Johnston RM, Iyer NA, Ngo TT, Dionne H, Abbott LF, Axel R, Tanimoto H, Rubin GM. 2014a. The neuronal architecture of the mushroom body provides a logic for associative learning. *eLife 2014*, **3**:e04577 DOI: 10.7554/eLife.04577

Aso Y, Sitaraman D, Ichinose T, Kaun KR, Vogt K, Belliart-Guérin G, Plac¸ ais PY, Robie AA, Yamagata N, Schnaitmann C, Rowell WJ, Johnston RM, Ngo TT, Chen N, Korff W, Nitabach MN, Heberlein U, Preat T, Branson KM, Tanimoto H, et al. 2014b. Mushroom body output neurons encode valence and guide memory-based action selection in *Drosophila*. *eLife* **3**:e04580. DOI: https://doi.org/10.7554/eLife.04580, PMID: 25535794

Bellonci G. 1882. Nuove ricerche Sulla struttura del ganglio ottico della Squilla mantis. *Memorie Della Accademia Delle Scienze dell'Istituto Di Bologna, Serie 4 Tomo* **3**:419–426.

Bethe A. 1897. Das Nervensystem von *Carcinus Maenas*. Ein anatomisch-physiologischer Versuch. *Archiv für mikroskopische Anatomie* **50**: 460–546; *Archiv für mikroskopische Anatomie* **51**:382–452

Bingman VP, Muzio RN. 2017. Reflections on the structural-functional evolution of the hippocampus: what is the big deal about a dentate gyrus? *Brain Behavior and Evolution* **90**:53–61. DOI: 10.1159/000475592

Bodian D. 1936. A new method for staining nerve fibers and nerve endings in mounted paraffin sections. *Anatomical Record* **65**:89–97. https://doi.org/10.1002/ar.1090650110

Brauchle M, Kiontke K, MacMenamin P, Fitch DHA, Piano F. 2009. Evolution of early embryogenesis in rhabditid nematodes. *Developmental Biology* **335**:253–262. https://doi.org/10.1016/j.ydbio.2009.07.033

Bridi JC, Ludlow ZN, Kottler B, Hartmann B, Broeck LV, Dearlove J, Göker M, Strausfeld NJ, Callaerts P, Hirth F. 2020. Ancestral regulatory mechanisms specify conserved midbrain circuitry in arthropods and vertebrates. *PNAS* **117**:19544-19555. DOI: 10.1073/pnas.1918797117

Buehlmann C, Wozniak B, Goulard R, Webb B, Graham P, Niven JE. 2020 Mushroom bodies are required for learned visual navigation, but not for innate visual behavior, in ants. *Current Biology* **23**. https://doi.org/10.1016/j.cub.2020.07.013

Cardona A, Saalfeld S, Schindelin J, Arganda-Carreras I, Preibisch S, Longair M, ... Douglas RJ. 2012. TrakEM2 software for neural circuit reconstruction. *PloS one* **7**:e38011. DOI: 10.1371/journal.pone.0038011

Clark RE, Broadbent NJ, Squire LR. 2005. Impaired remote spatial memory after hippocampal lesions despite extensive training beginning early in life. *Hippocampus* **15**:340–346. doi:10.1002/hipo.20076

Cournil I, Helluy SM, Beltz BS. 1994. Dopamine in the lobster *Homarus gammarus*. I. Comparative analysis of dopamine and tyrosine hydroxylase immunoreactivities in the nervous system of the juvenile. *Journal of Comparative Neurology* **334**:455–469. https://doi.org/10.1002/cne.903440308

Crisp KM, Klukas KA, Gilchrist LS, Nartey AJ, Mesce KA. 2001. Distribution and development of dopamine- and octopaminesynthesizing neurons in the medicinal leech. *Journal of Comparative Neurology* **442**:115–129. https://doi.org/10.1002/cne.10077

Davies R, Gagen MH, Bull JC, Pope EC. 2019. Maze learning and memory in a decapod crustacean. *Biology Letters* **1520190407**. http://doi.org/10.1098/rsbl.2019.0407

Day LB, Crews D, Wilczynski W. (2001. Effects of medial and dorsal cortex lesions on spatial memory in lizards, *Behaviour Brain Research* **118**:27–42.

Ehmer B, Gronenberg W. 2002. Segregation of visual input to the mushroom bodies in the honeybee (Apis mellifera). *Journal of Comparative Neurology* 451:362–373. doi:10.1002/cne.10355

Farris SM. 2005. Developmental organization of the mushroom bodies of *Thermobia domestica* (Zygentoma, Lepismatidae): insights into mushroom body evolution from a basal insect. *Evolution & Development* **7**:150–159. doi:10.1111/j.1525-142X.2005.05017.x

Farris SM. 2011. Are mushroom bodies cerebellum-like structures? *Arthropod Structure & Development* **40**:368-379. https://doi.org/10.1016/j.asd.2011.02.004

Farris SM, Schulmeister S. 2011. Parasitoidism, not sociality, is associated with the evolution of elaborate mushroom bodies in the brains of hymenopteran insects. *Proceedings of the Royal Society B*. **278**:940–951. http://doi.org/10.1098/rspb.2010.2161

Farris M, Strausfeld NJ. 2003. A unique mushroom body substructure common to basal cockroaches and to termites. *Journal of Comparative Neurology* **456**:305–320. doi:10.1002/cne.10517

Farris SM, Abrams AI, Strausfeld NJ. 2004. Development and morphology of Class II Kenyon cells in the mushroom bodies of the honey bee, *Apis mellifera*. *Journal of Comparative Neurology* **474**:325-339. doi:10.1002/cne.20146

Groh C, Rössler W. 2011. Comparison of microglomerular structures in the mushroom body calyx of neopteran insects. *Arthropod Structure & Development* **40**:358-367. https://doi.org/10.1016/j.asd.2010.12.002

Gronenberg W. 2001. Subdivisions of hymenopteran mushroom body calyces by their afferent supply. *The Journal of Comparative Neurology* **435**: 474-489. doi:10.1002/cne.1045

Guinot D. 2019. New hypotheses concerning the earliest brachyurans (Crustacea, Decapoda, Brachyura) *Geodiversitas* **41**:747-796. https://doi.org/10.5252/geodiversitas2019v41a22

Hamanaka Y, Mizunami M. 2019. Tyrosine hydroxylase-immunoreactive neurons in the mushroom body of the field cricket, *Gryllus bimaculatus*. *Cell Tissue Res* **376:**97–111. https://doi.org/10.1007/s00441-018-2969-9

Hamanaka Y, Minoura R, Nishino H, Miura T, Mizunami M. 2016) Dopamine- and tyrosine hydroxylase-immunoreactive neurons in the brain of the american cockroach, *Periplaneta americana*. *PLoS One* **11**:e0160531. doi: 10.1371/journal.pone.0160531

Hartnell RG. 1988. Evolution, systematics and geographical distribution. In: *Biology of the land crabs* (WW Burggren, BR McMahon, eds). Cambridge UP, Cambridge New York, Sydney. Pp. 6–54

Harzsch S, Anger K, Dawirs RR. 1997. Immunocytochemical detection of acetylated α-tubulin and *Drosophila* synapsin in the embryonic crustacean nervous system. *International Journal of Developmental Biology* **41**:477–484.

Harzsch S, Dawirs RR. 1996. Neurogenesis in the developing crab brain: Postembryonic generation of neurons persists beyond metamorphosis. *Journal of Neurobiology* **29**:384–398. doi:10.1002/(SICI)1097-4695(199603)29:3<384::AID-NEU9>3.0.CO;2-5

Harzsch S, Hansson BS. 2008. Brain architecture in the terrestrial hermit crab Coenobita clypeatus(Anomura, Coenobitidae), a crustacean with a good aerial sense of smell. *BMC Neuroscience* **9**:58. DOI: https://doi.org/ 10.1186/1471-2202-9-58

Harzsch S, Waloszeck D. 2000. Serotonin-immunoreactive neurons in the ventral nerve cord of Crustacea: A character to study aspects of arthropod phylogeny. *Arthropod Structure & Development* **29**:307–322. https://doi.org/10.1016/S1467-8039(01)00015-9

Healy SD Krebs JR. 1992. Food storing and the hippocampus in corvids: amount and volume are correlated. *Proceedings of the Royal Society of London B* **248**:241–245 http://doi.org/10.1098/rspb.1992.0068

Heuer CM, Loesel R. 2009. Three-dimensional reconstruction of mushroom body neuropils in the polychaete species *Nereis diversicolor* and *Harmothoe areolata* (Phyllodocida, Annelida). *Zoomorphology* **128**:219–226.DOI 10.1007/s00435-008-0063-7

Hevner RF. 2016. Evolution of the mammalian dentate gyrus. *The Journal of Comparative Neurology* **524**:578–594. doi:10.1002/cne.23851

Ito K, Awano W, Suzuki K, Hiromi Y, Yamamoto D. 1997. The *Drosophila* mushroom body is a quadruple structure of clonal units each of which contains a virtually identical set of neurones and glial cells. *Development* **124**:761–771. PMID: 9043058

Ito K, Suzuki K, Estes P, Ramaswami M, Yamamoto D, Strausfeld NJ. 1998. The organization of extrinsic neurons and their implications in the functional roles of the mushroom bodies in *Drosophila melanogaster* Meigen. *Learning & Memory* **5**:52–77. PMID: 10454372

Ito K, Shinomiya K, Ito M, Armstrong JD, Boyan G, Hartenstein V, Harzsch S, Heisenberg M, Homberg U, Jenett A, Keshishian H, Restifo LL, Ro¨ ssler W, Simpson JH, Strausfeld NJ, Strauss R, Vosshall LB, Insect Brain Name Working Group. 2014. A systematic nomenclature for the insect brain. *Neuron* **81**:755–765. DOI: https://doi.org/10.1016/j.neuron.2013.12.017, PMID: 24559671

Jacob PF, Waddell S. 2020. Spaced training forms complementary long-term memories of opposite valence in *Drosophila*. *Neuron* **106**:977-991.e4. https://doi.org/10.1016/j.neuron.2020.03.013

Jacoby CA. 1981. Behavior of the Purple Shore Crab *Hemigrapsus nudus* Dana, 1851. *Journal of Crustacean Biology* **1**:531–544. https://doi.org/10.2307/1548130

Kalderon D, Rubin GM. 1988. Isolation and characterization of Drosophila cAMP-dependent protein kinase genes. *Genes & Development* **2**:1539–1556. DOI: https://doi.org/10.1101/gad.2.12a.1539, PMID: 3215511

Kamhi JF, Barron AB, Narendra A. (2020). Vertical lobes of the mushroom bodies are essential for view-based navigation in Australian bull ants. *Current Biology* **23**: https://doi.org/10.1016/j.cub.2020.06.030.

1304 Kanzaki R, Arbas EA, Strausfeld NJ, Hildebrand JG. 1989. Physiology and morphology of
1305 projection neurons in the antennal lobe of the male moth *Manduca sexta*. *Journal of*
1306 *Comparative Physiology A* **165**:427–453.
1307
1308 Kinoshita M. Shimohigasshi M, Tominaga Y, Arikawa K., Homberg, U. 2015. Topographically
1309 distinct visual and olfactory inputs to the mushroom body in the Swallowtail butterfly, *Papilio*
1310 *xuthus*. *Journal of Comparative Neurology* **523**:162–182. doi:10.1002/cne.23674
1311
1312 Klagges BR, Heimbeck G, Godenschwege TA, Hofbauer A, Pflugfelder GO, Reifegerste R. et
1313 al. 1996. Invertebrate synapsins: A single gene codes for several isoforms in *Drosophila*.
1314 *Journal of Neuroscience* **16**:3154–3165. https://doi.org/10.1523/JNEUROSCI.16-10-03154.1996
1315
1316 Krebs J, Sherry DFf, Healy SD, Perry VH, Vaccarino AL. 1989. Hippocampal specialization of
1317 food-storing birds (passerines/memory). *PNAS* **86:**1388–1392.
1318
1319 Lange AB, Chan K. 2008. Dopaminergic control of foregut contractions in *Locusta migratoria*.
1320 *Journal of Insect Physiology* **54**:222–230. https://doi.org/10.1016/j.jinsphys.2007.09.005
1321
1322 Lee SY. 2015. *Ecology of Brachyura*. In: Treatise on Zoology - Anatomy, Taxonomy, Biology.
1323 *The Crustacea* **9C**:469–541.DOI: https://doi.org/10.1163/9789004190832_011
1324
1325 Leitch B, Laurent G. 1996. GABAergic synapses in the antennal lobe and mushroom body of the
1326 locust olfactory system. *Journal of Comparative Neurology* **372**:487–514. doi:10.1002/(SICI)1096-
1327 9861(19960902)372:4<487::AID-CNE1>3.0.CO;2-0
1328
1329 Li F, Lindsey J, Marin EC, Otto N, Dreher M, Dempsey G, et al. (2020). The connectome of the
1330 adult *Drosophila* mushroom body: implications for function. BioRxiv. doi:
1331 https://doi.org/10.1101/2020.08.29.273276
1332
1333 Li Y, Strausfeld NJ. 1997. Morphology and sensory modality of mushroom body extrinsic
1334 neurons in the brain of the cockroach, *Periplaneta americana.The Journal of Comparative*
1335 *Neurology* **387**: 631-650. doi:10.1002/(SICI)1096-9861(19971103)387:4<631::AID-
1336 CNE9>3.0.CO;2-3
1337
1338 Li Y, Strausfeld NJ. 1999. Multimodal efferent and recurrent neurons in the medial lobes of
1339 cockroach mushroom bodies. *The Journal of Comparative Neurology* **409**:647–663. DOI:
1340 https://doi.org/10.1002/(SICI)1096-9861
1341
1342 Li J, Mahoney BD, Jacob MS, Caron SJC. 2020. Visual input into the *Drosophila*
1343 *melanogaster* mushroom body**.** *Cell Reports* **30:** https://doi.org/10.1016/j.celrep.2020.108138
1344
1345 Lin C, Strausfeld NJ. 2012. Visual inputs to the mushroom body calyces of the whirligig
1346 beetle *Dineutus sublineatus*: Modality switching in an insect. *The Journal of Comparative*
1347 *Neurology* **520**:2562-2574. doi:10.1002/cne.23092
1348
1349 Liu X, Davis R. 2009. The GABAergic anterior paired lateral neuron suppresses and is
1350 suppressed by olfactory learning. *Nature Neuroscencei* **12,** 53–59 (2009).
1351 https://doi.org/10.1038/nn.2235
1352

Liu C, Plaçais P, Yamagata N, Pfeiffer BD, Aso Y, et al. .2012. A subset of dopamine neurons signals reward for odour memory in *Drosophila*. *Nature* **488**:512–516. https://doi.org/10.1038/nature11304

López JC, Vargas JP, Gómez Y, Salas C. (2003) Spatial and non-spatial learning in turtles: the role of medial cortex, *Behaviour Brain Research* **143**:109–120.

Maza FJ, Sztarker J, Shkedy A, Peszano VN, Locatelli FF, Delorenzi A. 2016. Context-dependent memory traces in the crab's mushroom bodies: Functional support for a common origin of high-order memory centers. *Proceedings of the National Academy of Science USA* **113**:E7957–E7965. DOI: https://doi.org/10.1073/pnas.1612418113, PMID: 27856766

Maza FJ, Sztarker J, Cozzarin ME, Lepore MG, Delorenzi A. 2020. A crabs' high-order brain center resolved as a mushroom body-like structure. *The Journal of Comparative Neurology*. 2020:1– 23. https://doi.org/10.1002/cne.24960

McKinzie ME, Benton JJ, Beltz BS, Mellon DF Jr. 2003. Parasol cells of the hemiellipsoid body in the crayfish Procambarus clarkii: Dendritic branching patterns and functional implications. *Journal of Comparative Neurology* **462**:168–179. https://doi.org/10.1002/cne.10716

Mellon DF Jr., Alones V, Lawrence MD. 1992a. Anatomy and fine structure of neurons in the deutocerebral projection pathway of the crayfish olfactory system. *The Journal of Comparative Neurology* **321**:93–111. doi:10.1002/cne.903210109

Mellon DF Jr., Sandeman DC, Sandeman RE. 1992b. Characterization of oscillatory olfactory interneurons in the protocerebrum of the crayfish. *Journal of Experimental Biology* **167**:5–38.

Mizunami M, Weibrecht JM, Strausfeld NJ. 1998. Mushroom bodies of the cockroach: their participation in place memory. *The Journal of Comparative Neurology* **402**:520–537.

Molina Y, O'Donnell S.. 2007. Mushroom body volume is related to social aggression and ovary development in the paperwasp *Polistes instabilis. Brain Behavoir and Evolution* **70**:137–144. (doi:10.1159/000102975).

Molina Y, O'Donnell S. 2008Age, sex, and dominance-related mushroom body plasticity in the paper wasp *Mischocyttarus mastigophorus*. *Developmental Neurobiology* **68**:950–959. (doi:10.1002/dneu.20633).

Montgomery SH, Ott SR. 2015. Brain composition in *Godyris zavaleta*, a diurnal butterfly, reflects an increased reliance on olfactory information. *The Journal of Comparative Neurology* **523**:869–891. doi:10.1002/cne.23711

Montgomery SH, Merrill RM, Ott SR. 2016. Brain composition in *Heliconius* butterflies, posteclosion growth and experience-dependent neuropil plasticity. *The Journal of Comparative Neurology* **524**:1747–1769. DOI: https://doi. org/10.1002/cne.23993, PMID: 26918905

Modi MN, Shuai Y, Turner GC. 2020.The Drosophila mushroom body: from architecture to algorithm in a learning circuit. *Annual Review of Neuroscience* **43**:465–84. https://doi.org/10.1146/annurev-neuro-080317- 0621333

Nässel DR, Elekes K. 1992. Aminergic neurons in the brain of blowflies and Drosophila: dopamine- and tyrosine hydroxylase-immunoreactive neurons and their relationship with putative histaminergic neurons. *Cell & Tissue Research* **267**:147–167. DOI: https://doi.org/10.1007/BF00318701, PMID: 1346506

Ng PKL, Guinot D, Davie PJF. 2008. Systema brachyurorum: part I. an annotated checklist of extant brachyuran crabs of the world. *Raffles Bulletin of Zoology Supplement Series* **17**:1–286.

Okamura JY, Strausfeld NJ. 2007. Visual system of calliphorid flies: Motion- and orientation-sensitive visual interneurons supplying dorsal optic glomeruli. *Journal of Comparative Neurology* **500**:189–205. https://doi.org/10.1002/cne.21195

Owald D, Felsenberg J, Talbot CB, Das G, Perisse E, Huetteroth W, Waddell S. 2015. Activity of defined mushroom body output neurons underlies learned olfactory behavior in Drosophila. *Neuron* **86**:417–427. DOI: https://doi.org/10.1016/j.neuron.2015.03.025, PMID: 25864636

Phillips-Portillo J, Strausfeld NJ. 2012. Representation of the brain's superior protocerebrum of the flesh fly, *Neobellieria bullata*, in the central body. *Journal of Comparative Neurology* **520**:3070–3087. doi:10.1002/cne.23094

Ott SR, Rogers SM. 2010. Gregarious desert locusts have substantially larger brains with altered proportions compared with the solitarious phase. *Proceedings of the Royal Society B* **277**:3087–3096

Patel RN, Cronin TW. 2020. Mantis shrimp navigate home using celestial and idiothetic path integration. *Current Biology* **30**:1981–1987. https://doi.org/10.1016/j.cub.2020.03.023

Perisse E, Yin Y, Lin AC, Lin S, Huetteroth W, Waddell S. 2013. Different Kenyon cell populations drive learned approach and avoidance in *Drosophila*. *Neuron* **79**:945-956. (doi:10.1016/J.NEURON.2013.07.045)

Salas C, Broglio C, Rodriguez F .2003. Evolution of forebrain and spatial cognition in vertebrates: conservation across diversity. *Brain, Behavior and Evolution* **62**:72–82.

Sandeman DC, Scholtz G, Sandeman RE. 1993. Brain evolution in decapod crustacea. *Journal of Experimental Zoology* **265**:112–133. DOI: https://doi.org/10.1002/jez.1402650204

Sayre ME, Strausfeld NJ. 2019. Mushroom bodies in crustaceans: Insect-like organization in the caridid shrimp *Lebbeus groenlandicus*. *Journal of Comparative Neurology* **527**:2371–2387. DOI: https://doi.org/10.1002/cne.24678

Schürmann F-W. 1987. The architecture of the mushroom bodies and related neuropils in the insect brain. In: *Arthropod Brain: Its Evolution, Development, Structure, and Functions* (ed. A.P. Gupta). John Wiley & Sons, New York. 231-264.

Schweitzer CE, Feldmann RM. 2010. The oldest Brachyura (Decapoda: Homolodromioidea: Glaessneropsoidea) known to date (Jurassic). *Journal of Crustacean Biology* **30**:251-256.

1451 Sinakevitch I, Farris SM, Strausfeld NJ. 2001. Taurine-, aspartate- and glutamate-like
1452 immunoreactivity identifies chemically distinct subdivision of Kenyon cells in the cockroach
1453 mushroom body. *Journal of Comparative Neurology* **439**: 352–367. doi:10.1002/cne.1355
1454
1455 Sintoni S, Fabritius-Vilpoux K, Harzsch S. 2007. The engrailed-expressing secondary head
1456 spots in the embryonic crayfish brain: Examples for a group of homologous neurons in
1457 Crustacea and Hexapoda? *Development Genes & Evolution* **217**:791– 799.
1458 https://doi.org/10.1007/s00427-007-0189-5
1459
1460 Sjöholm M, Sinakevitch I, Ignell R, Strausfeld NJ, Hansson BS. 2005. Organization of Kenyon
1461 cells in subdivisions of the mushroom bodies of a lepidopteran insect. *Journal of Comparative*
1462 *Neurology* **491**: 290-304. doi:10.1002/cne.20698
1463
1464 Sjöholm M, Sinakevitch I, Strausfeld NJ, Ignell R, Hansson BS. 2006. Functional division of
1465 intrinsic neurons in the mushroom bodies of male *Spodoptera littoralis* revealed by antibodies
1466 against aspartate, taurine, FMRF-amide, Mas-allatotropin and DC0. *Arthropod Structure &*
1467 *Development* **35**:153-168. https://doi.org/10.1016/j.asd.2006.03.001
1468
1469 Skoulakis EMC, Kalderon D, Davis RL. 1993. Preferential expression in mushroom bodies of
1470 the catalytic subunit of protein kinase a and its role in learning and memory. *Neuron* **11**:197–
1471 208. https://doi. org/10.1016/0896-6273(93)90178-T
1472
1473 Stegner ME, Richter S. 2011. Morphology of the brain in *Hutchinsoniella macracantha*
1474 (Cephalocarida, crustacea). *Arthropod Structure & Development* **40**:221–243. DOI:
1475 https://doi.org/10.1016/j.asd.2011.04.001, PMID: 21679884
1476
1477 Stemme T, Iliffe TM, Bicker G. 2016. Olfactory pathway in *Xibalbanus tulumensis*: Remipedian
1478 hemiellipsoid body as homologue of hexapod mushroom body. *Cell and Tissue Research*
1479 **363**:635–648. https://doi.org/10.1007/s00441-015-2275-8
1480
1481 Stern M. 2009. The PM1 neurons, movement sensitive centrifugal visual brain neurons in the
1482 locust: Anatomy, physiology, and modulation by identified octopaminergic neurons. *Journal of*
1483 *Comparative Physiology A* **195**:123–137. https://doi.org/10.1007/s00359-008-0392-5
1484
1485 Striedter GF. 2016. Evolution of the hippocampus in reptiles and birds. *Journal of Comparative*
1486 *Neurology* **524**:496-517. doi:10.1002/cne.23803
1487
1488 Strausfeld NJ. 2012. Arthropod Brains: Evolution, Functional Elegance, and Historical
1489 Significance. Boston, MA: Harvard Belknap Press.
1490
1491 Strausfeld NJ. 2002. Organization of the honey bee mushroom body: Representation of the
1492 calyx within the vertical and gamma lobes. *Journal of Comparative Neurology* **450**:4-33.
1493 doi:10.1002/cne.10285
1494
1495 Strausfeld NJ. 2020. Nomen est omen, cognitive dissonance and homology of memory centers
1496 in crustaceans and insects. *Journal of Comparative Neurology*. doi:10.1002/cne.24919
1497
1498 Strausfeld NJ, Li Y. 1999. Representation of the calyces in the medial and vertical lobes of
1499 cockroach mushroom bodies. *Journal of Comparative Neurology* **409**:626–646.
1500 doi:10.1002/(SICI)1096-9861(19990712)409:4<626::AID-CNE8>3.0.CO;2-B

1501
1502 Strausfeld NJ, Sayre ME. 2020. Mushroom bodies in Reptantia reflect a major transition in
1503 crustacean brain evolution. *Journal of Comparative Neurology* **528**:261–282.
1504 https://doi.org/10.1002/cne. 24752
1505
1506 Strausfeld, N. J., Wolff, G. H., & Sayre, M. E. (2020). Mushroom body evolution demonstrates
1507 homology and divergence across Pancrustacea. *eLife* **9** (e52411), 1–46.
1508 https://doi.org/10.7554/eLife. 52411
1509
1510 Strausfeld NJ, Sinakevitch I, Brown SM, Farris SM. 2009. Ground plan of the insect mushroom
1511 body: functional and evolutionary implications. *Journal of Comparative Neurology* **513**:265–291.
1512 DOI: https://doi.org/10.1002/cne.21948, PMID: 19152379
1513
1514 Strausfeld NJ, Hansen L, Li Y, Gomez RS, Ito K. 1998. Evolution, discovery, and interpretations
1515 of arthropod mushroom bodies. *Learning & Memory* **5**:11–37. (doi:10.1101/lm.5.1.11)
1516
1517 Strausfeld NJ, Sinakevitch I, Vilinsky, I. 2003. The mushroom bodies of *Drosophila*
1518 *melanogaster*: an immunocytological and Golgi study of Kenyon cell organization in the calyces
1519 and lobes. *Microscopy Research and Technique* **62**:151–169.
1520
1521 Sullivan JM, Benton JL, Sandeman DC, Beltz BS. 2007. Adult neurogenesis: A common
1522 strategy across diverse species. *Journal of Comparative Neurology* **500**:574–584.
1523 https://doi.org/10.1002/cne.21187
1524
1525 Suryanarayana SM, Robertson B, Wallén P, Grillner S. 2017. The lamprey pallium provides a
1526 blueprint of the mammalian layered cortex. *Current Biology* **27**:3264–3277.
1527 https://doi.org/10.1016/j.cub.2017.09.034
1528
1529 Tanaka, N.K., Tanimoto, H. and Ito, K. (2008), Neuronal assemblies of the Drosophila
1530 mushroom body. *Journal of Comparative Neurology* **508**:711–755. doi:10.1002/cne.21692
1531
1532 Tanner CJ, Jackson AL. 2012. Social structure emerges via the interaction between
1533 local ecology and individual behaviour. *Journal of Animal Ecology* **81**:260-267 doi: 10.1 1 1 1/j.
1534 1 365-2656.201 1 .01879.x
1535
1536 Tedjakumala SSR, Rouquette J, Boizeau M-L, Mesce KA, Hotier L, Massou I, Giurfa. 2017.
1537 Tyrosine-hydroxylase characterization of dopaminergic neurons in the honey bee brain.
1538 *Frontiers in Systems Neuroscience* **11**:47.
1539 https://www.frontiersin.org/article/10.3389/fnsys.2017.00047
1540
1541 Thazhath R, Liu C, Gaertig J.2002. Polyglycylation domain of β-tubulin maintains axonemal
1542 architecture and affects cytokinesis in Tetrahymena. *Nature Cell Biology* **4**:256–259.
1543 https://doi.org/10. 1038/ncb764
1544
1545 Tosches MA, Yamawaki TM, Naumann RK, Jacobi AA, Tushev G, Laurent G. 2018. Evolution of
1546 pallium, hippocampus, and cortical cell types revealed by single-cell transcriptomics in reptiles.
1547 *Science* **360**:881–888.
1548
1549 Tomer R, Denes AS, Tessmar-Raible K, Arendt D. 2010. Profiling by image registration reveals

common origin of annelid mushroom bodies and vertebrate pallium. *Cell* **142**:800–809. doi:10.1016/j.cell.2010.07.043.

Traniello IM, Chen Z, Bagchi VA, Robinson GE. 2019. Valence of social information is encoded in different subpopulations of mushroom body Kenyon cells in the honeybee brain. *Proceedings of the Royal Society **B*** 286:20190901. http://dx.doi.org/10.1098/rspb.2019.0901

Turner GC, Bazhenov M, Laurent G. 2008. Olfactory representations by Drosophila mushroom body neurons. *Journal of Neurophysiology* **99**:734–746. https://doi.org/10.1152/jn.01283.2007

Vargas JP, Rodríguez F, López JC, Arias JL, Salas C. 2000.Spatial learning-induced increase in the argyrophilic nucleolar organizer region of dorsolateral telencephalic neurons in goldfish. *Brain Research* **865**:77–84.

van Dijk LJA, Janz N, Schäpers A, Gamberale-Stille G, Carlsson MA. 2017. Experience-dependent mushroom body plasticity in butterflies: consequences of search complexity and host range. *Proceedings of the Royal Society B* **284**:20171594. http://dx.doi.org/10.1098/rspb.2017.1594

Vogt K, Aso Y, Hige T, Knapek S, et al. 2016. Direct neural pathways convey distinct visual information to *Drosophila* mushroom bodies. *eLife 2016* **5**:e14009 DOI: 10.7554/eLife.14009

Wigglesworth VB. 1957. The use of osmium in the fixation and staining of tissues. *Proceedings of the Royal Society B* **147**:185–199. https://doi.org/10.1098/rspb.1957.0043

Withers GS, Fahrbach SE, Robinson GE. 1993. Selective neuroanatomical plasticity and division of labour in the honeybee. *Nature* **364**:238–240. doi:10.1038/364238a0

Withers G, Day NF, Talbot EF, Dobson HEM, Wallace CS. 2008. Experience-dependent plasticity in the mushroom bodies of the solitary bee *Osmia lignaria* (Megachilidae). *Developmental Neurobiology* **68**:73–82. doi:10.1002/dneu.20574.

Wolfe JM, Breinholt JW, Crandall KA, Lemmon AR, Lemmon EM, Timm LE, Siddall ME, Bracken-Grissom HD. 2019. A phylogenomic framework, evolutionary timeline and genomic resources for comparative studies of decapod crustaceans. *Proceedings of the Royal Society B*: *Biological Sciences* **286**:20190079. DOI: https://doi.org/10.1098/rspb.2019.0079

Wolff G, Harzsch S, Hansson BS, Brown S, Strausfeld N. 2012. Neuronal organization of the hemiellipsoid body of the land hermit crab, *Coenobita clypeatus*: correspondence with the mushroom body ground pattern. *Journal of Comparative Neurology* **520**:2824–2846. DOI: https://doi.org/10.1002/cne.23059, PMID: 22547177

Wolff GH, Thoen HH, Marshall J, Sayre ME, Strausfeld NJ. 2017. An insect-like mushroom body in a crustacean brain. *eLife* **6**:e29889. DOI: https://doi.org/10.7554/eLife.29889, PMID: 28949916

Wolff GH, Strausfeld NJ. 2015. Genealogical correspondence of mushroom bodies across invertebrate phyla. *Current Biology* **25**:38–44. DOI: https://doi.org/10.1016/j.cub.2014.10.049, PMID: 25532890

Wolff GH, Strausfeld NJ. 2016. Genealogical correspondence of a forebrain centre implies an executive brain in the protostome–deuterostome bilaterian ancestor. *Philosophical Transactions of the Royal Society B: Biological Sciences* **371**:20150055. DOI: https://doi.org/10.1098/rstb.2015.0055

Yagi R, Mabuchi Y, Mizunami M, Tanaka NK. 2016. Convergence of multimodal sensory pathways to the mushroom body calyx in *Drosophila melanogaster. Scientific Reports* **6**:29481. DOI: 10.1038/srep29481

Yasuyama K, Meinertzhagen IA, Schürmann F-W. 2002. Synaptic organization of the mushroom body calyx in *Drosophila melanogaster*. *Journal of Comparative Neurology* **445**:211–226. doi:10.1002/cne.10155

Terminology

Terms and abbreviations follow recommendations by the insect brain consortium regarding those jointly applicable to insect and crustacean (Pancrustacea) central nervous systems. See Ito et al. (2014). Other terms used for crustacean brain centers follow those of Bellonci (1882) and Sandeman et al. (1993). Other terms are defined in the body of this paper.

Acknowledgements

The research described here is supported by the National Science Foundation under Grants No. 1754798 awarded to NJS. Our gratitude is once again directed to Daniel Kalderon, Columbia University, New York, for supplying the DC0 antibodies, as he has during the last decade and longer. We thank the staff of the University of Washington's Friday Harbor Marine Laboratories, San Juan, for their unfailing help in obtaining living specimens. Briana Olea-Rowe and Hannah Joy Miller provided expert technical assistance. We have profited from discussions and advice from Wulfila Gronenberg (University of Arizona) and Frank Hirth (Kings College, University of London) and are indebted to Camilla Strausfeld for her advice, critically discussing versions of the manuscript, suggesting many improvements and meticulously editing the text.

FIGURE SUPPLEMENTS

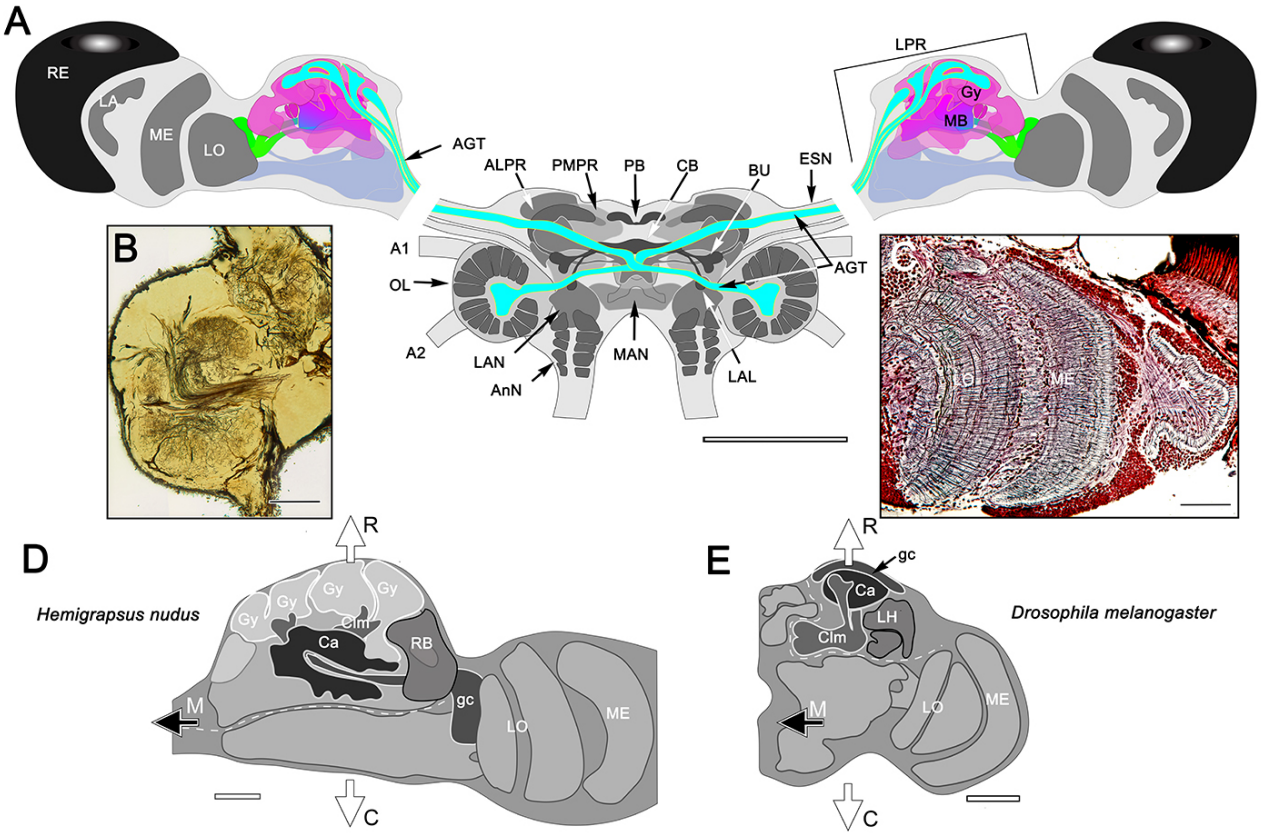

Figure 1 —— figure supplement 1. (**A**) Schematic of the *Hemigrapsus* brain (frontal view) and major neuropils. Abbreviations: ALPR, anterior lateral protocerebrum; A1, antennule nerve; A2, antennal nerve; AnN, antenna 2 neuropil; BU, lateral bulb of the central complex; CB, central body; ESN, eyestalk nerve; LAL, lateral accessory lobe; LAN, lateral antennular lobe neuropil; LA, lamina; LO, lobula; LPR, lateral protocerebrum; MAN, medial antenna 1 neuropil; MB, mushroom body; ME, medulla; OL, olfactory lobe; OGT, olfactory globular tract; PMPR, posterior medial protocerebral neuropils; PB, protocerebral bridge; RE, compound retina. The eyestalk nerve ESN) carries *all* axons connecting the brain with the lateral protocerebrum. (**B**) Example of mass Golgi impregnation showing the olfactory lobe and origin of the OGT. (**C**) Reduced silver sections resolve neuroarchitecture, here of the optic lobe medulla and lobula. (**D, E**) Orientations of the varunid lateral protocerebrum aligned with that of *Drosophila*. The white dashed lines in *H. nudu*s divides its rostral lateral protocerebral volume from its caudal volume; in Drosophila the dashed line divides the rostral volume of the protocerebrum from the rest of the hemi-brain. In both taxa the filled arrow M indicates the medial, the open arrows R and C indicate, respectively, the rostral and caudal axes. These conventions are used throughout this account. Both schematics depict a view from the ventral side of the lateral protocerebrum/ hemibrain. Abbreviations: Ca, calyces; Clm, column; gc, globuli cells; Gy, gyri; LH, lateral horn; LO, lobula complex; ME, medulla; RB, reniform body; Scale bars, A, 500μm; B–D 100μm

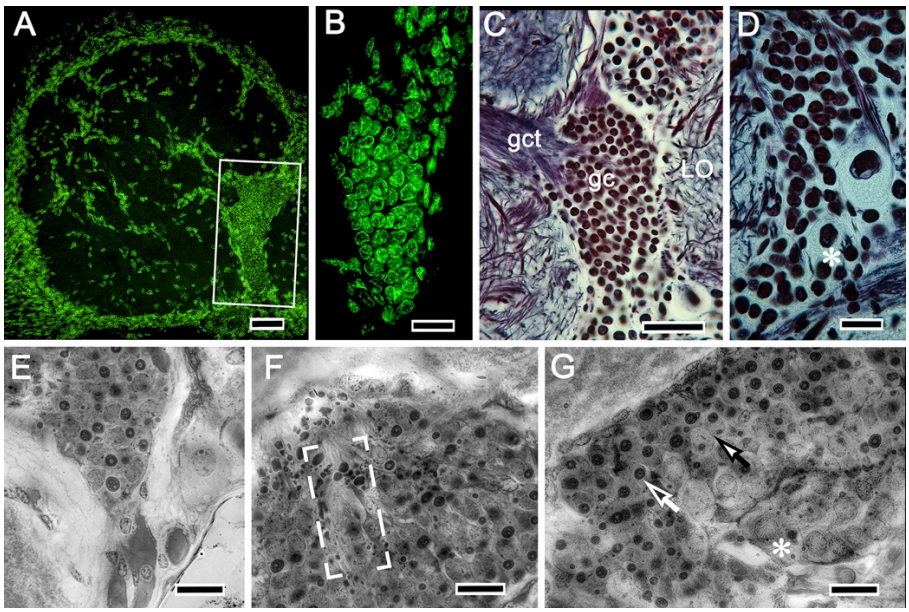

Figure 2 —— figure supplement 1. Globuli cells supplying intrinsic neurons to the mushroom bodies. In the varunid crab, globuli cells occupy a unique location between the distal margin of the lateral protocerebrum and proximal margin of the optic lobe as shown in **A**. (**B**) As is typical of globuli cells in other taxa (insects, shrimps) they are minute, here measuring less than 6 μm diameter, the next largest being reniform perikarya as in panel C, upper right. (**D-G**) Like other decapods, crabs molt and grow throughout life, their brains also increasing in size. The globuli cell cluster evidences neuroblasts (asterisk in panel D), and grouped globuli cells suggesting clonal siblings (**E**). Ganglion mother cells are also arranged as aligned groups (**F**) or, as in panel **G**, dividing (closed arrow) between neuroblasts (asterisk) and fully differentiated perikarya (open arrow). Scale bars, A, 50mm; B, 20μm; C, 50μm; D-G, 20μm.

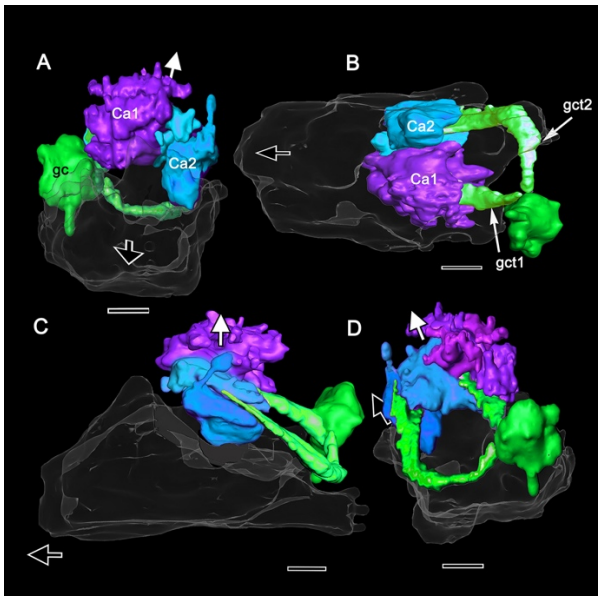

Figure 2 —— figure supplement 2. Globuli cells provide two tracts, one to each calyx as shown in this Amira reconstruction of a serially sectioned osmium-ethyl gallate-treated brain. Two tracts composed of neurites from 2,000-3,000 globuli cells from a unified cluster (gc) extend to two calyces (Ca1, Ca2), Ca1 is dorsal to and larger than Ca2. (**A**) Viewed from above, with the medial margin of the lateral protocerebrum

closest to the observer, the rostral surfaces of each calyx are highly indented with some finger-like extensions reaching upwards. (**B**) viewed from beneath, with the dorsal calyx 1 closest to the observer, the more caudal levels of the calyces are seen to be layered, this distinction between caudal and rostral volumes also shown viewing into the lateral protocerebrum from its ventral surface (C). (**D**) 180º rotation from panel A suggests greater surface elaboration of Ca1 than Ca2.

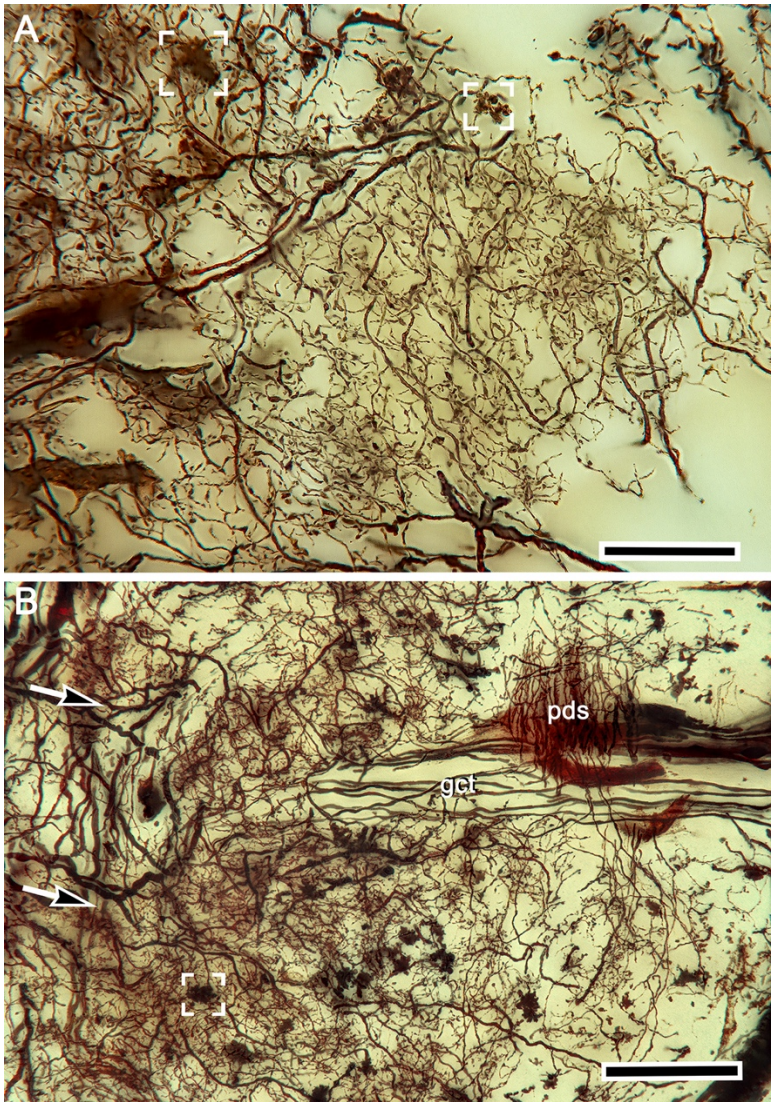

Figure 3 —— figure supplement 1. Rectilinear network organization of the calyx and afferent supply. (**A**) Golgi impregnation showing regular network arrangements of intrinsic cell dendrites. Robust afferent terminals are defined by varicose specializations. A single terminal is shown in the box upper right; several convergent terminals in the box upper left. (**B**) The globuli cell tract (gct) extends medially beneath processes belonging to the reniform body's pedestal (pds). Afferent terminals fibers enter from the left (arrowed) to distribute terminals (one boxed, lower left) amongst densely arranged intrinsic neuron dendrites extending from globuli cell neurites comprising the gct. Scale bars, A, B, 50μm.

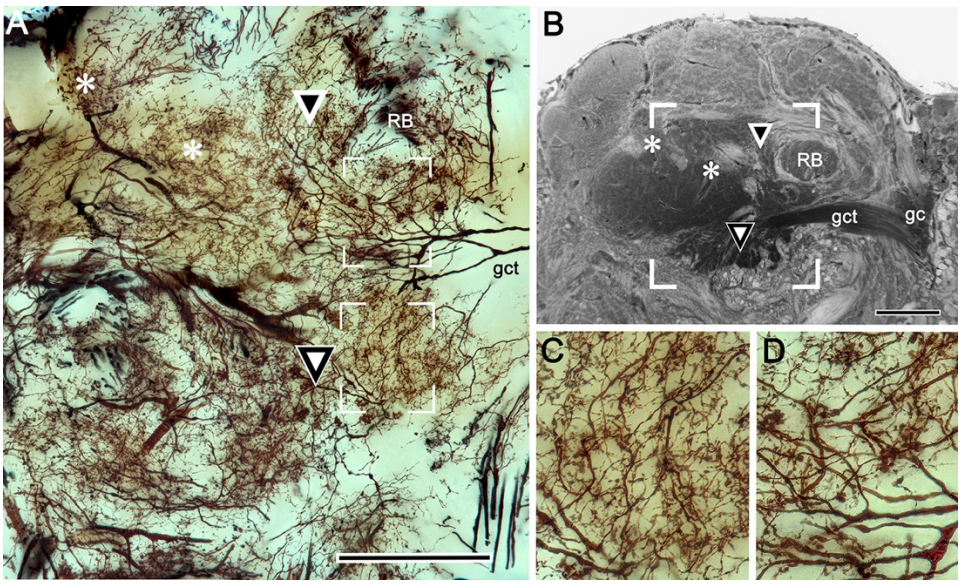

Figure 4 —— figure supplement 1. Fidelity of intrinsic neurons fields (**A**) and calycal domains revealed by osmium-ethyl gallate (**B**). The equivalent of the area in panel **A** is indicated by the open box in panel **B**. Corresponding loci in B and A are indicated by symbols. Boxed areas in **A** are enlarged in panels **C**, **D** showing rectilinear organization of intrinsic processes and their convergence at nodes corresponding to microglomeruli. Abbreviations: RB, reniform pedestal; gc, globuli cells; gct, globuli cell tract. Scale bars, A, B, 100μm

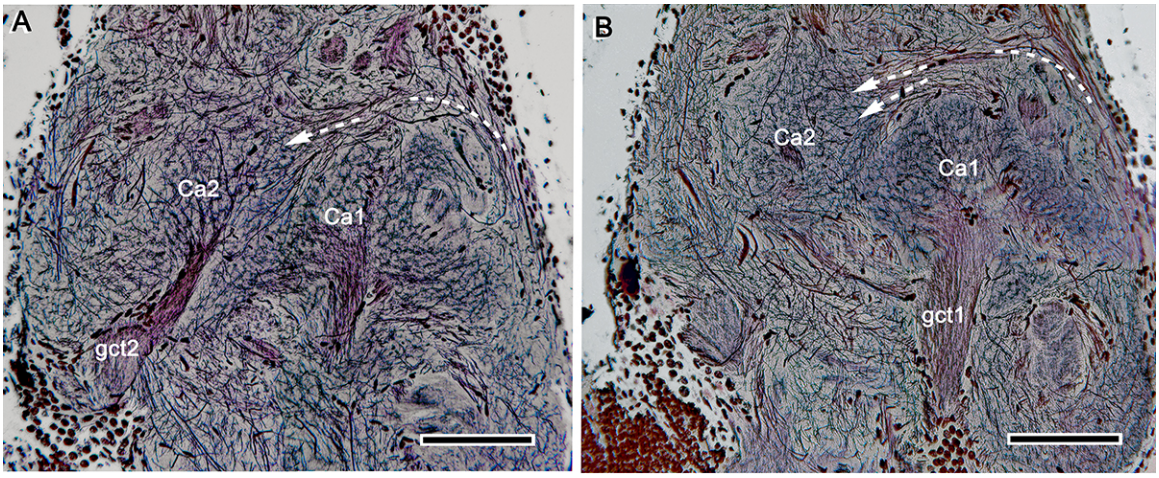

Figure 4 —— figure supplement 2. Calyx distinctions. (**A, B**) Two serial silver-stained sections showing the side-by-side disposition of calyces 1, 2 (Ca1, Ca2) each supplied by its own globuli cell tract (gct1, 2). Arrowed paths indicate passage of axons extending to Ca2 from pathways from the optic lobe medulla and reniform body (far right in both panels). Scale bars, 100μm.

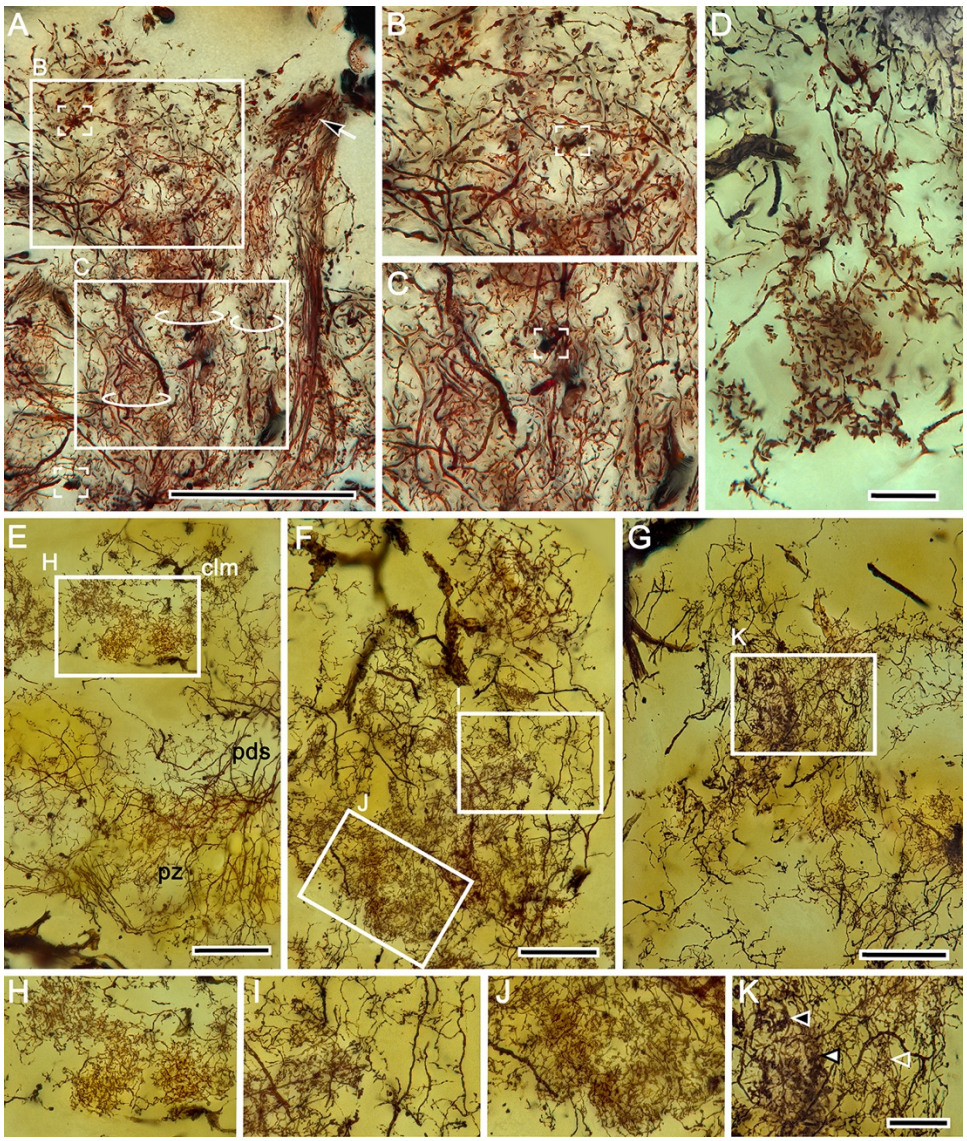

Figure 7 —— figure supplement 1. Intrinsic neuron organization in columns. (**A**) Golgi impregnation of a column originating from calyx 2. Three parallel but distinct ensembles of intrinsic neuron processes (circled) all splay outwards immediately beneath the overlying gyriform neuropil, which is here unstained. Details of these ensembles shown in **B**, **C** demonstrate internal complexity. Of note is the presence of bouton-like terminals (two indicated by box brackets) suggesting either afferent supply from the eyestalk nerve or reciprocal inputs from rostral gyri. A cascade arrangement of processes extending parallel to the column from a more rostral level (arrow) may indicate recurrent afferent supply from the gyri. (**D–G**) Columns also contain what appear to be intrinsic elements (**D**) that do not originate from the calyces, as occurs in the mushroom bodies of certain insects (see Discussion). (**E**) There is a clear distinction between the arrangement of processes (enlarged in **H**) in the columns (clm) and the more distributed arrangements in the proximal zone (pz) of the reniform body indicated by its pedestal (pds). (**F**) Further complexity is demonstrated by parallel arrangements of intrinsic neuron and their collaterals suggestive of local circuits (examples indicated in boxed areas in panel F, enlarged in **I**, **J**). (**G**) Dense arrangements near the column's terminal expansion reveal claw-like specializations each with its particular morphology, within parallel subdivisions of the column (indicated by arrowheads in K). Scale bars, A,100μm; E–G, 25μm; D, H-K, 20μm.

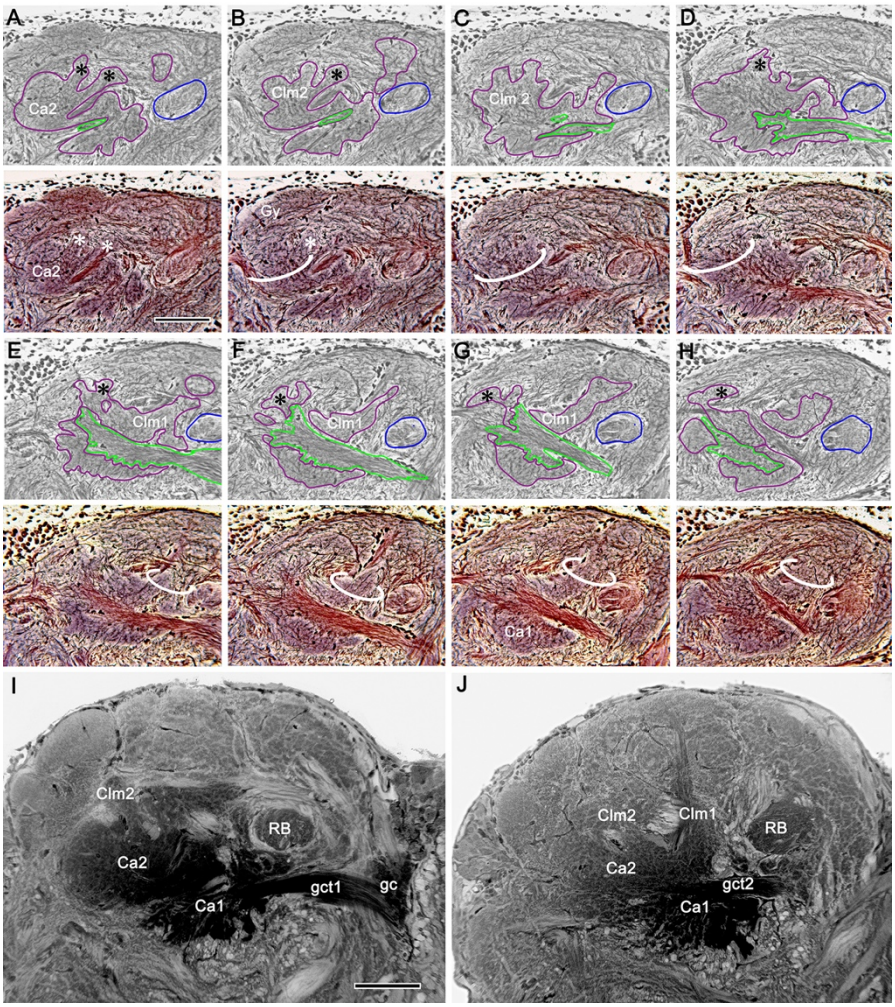

Figure 7 —— figure supplement 2. The interface between columns and gyri. (**A-H**) Paired half-tone/color micrographs of selected levels of a silver-stained, serially sectioned RLPR (medial to the left, rostral upwards). Green outlines in panels A-D indicate parts of the globuli cell tract (gct2) to calyx 2 (Ca2); in E-H, parts of the gct1 to calyx 1 (Ca1). Blue outlines indicate cross–sections of the reniform body pedestal (RB); magenta outlines indicate mushroom bodies (calyces and their columns). Identification of the calyces is enabled by their color and microglomeruli as in Ca2, (lower panel A). As in osmium-ethyl gallate sections, the two calyces are too close to identify separately unless viewed downwards from the rostral surface of the LPR (as in Figure 4 - figure supplement 2). Columns (ringed) and smaller finger-like extensions (asterisks) extend outwards to the gyri. Column 2 (Clm2) from calyx 2 (Ca2) is shown in panels A-D. Panels E-H illustrate the origin and width of Clm1 from Ca1. Panels I and J show corresponding arrangements revealed by osmium-ethyl gallate. Scale bars, 100μm.

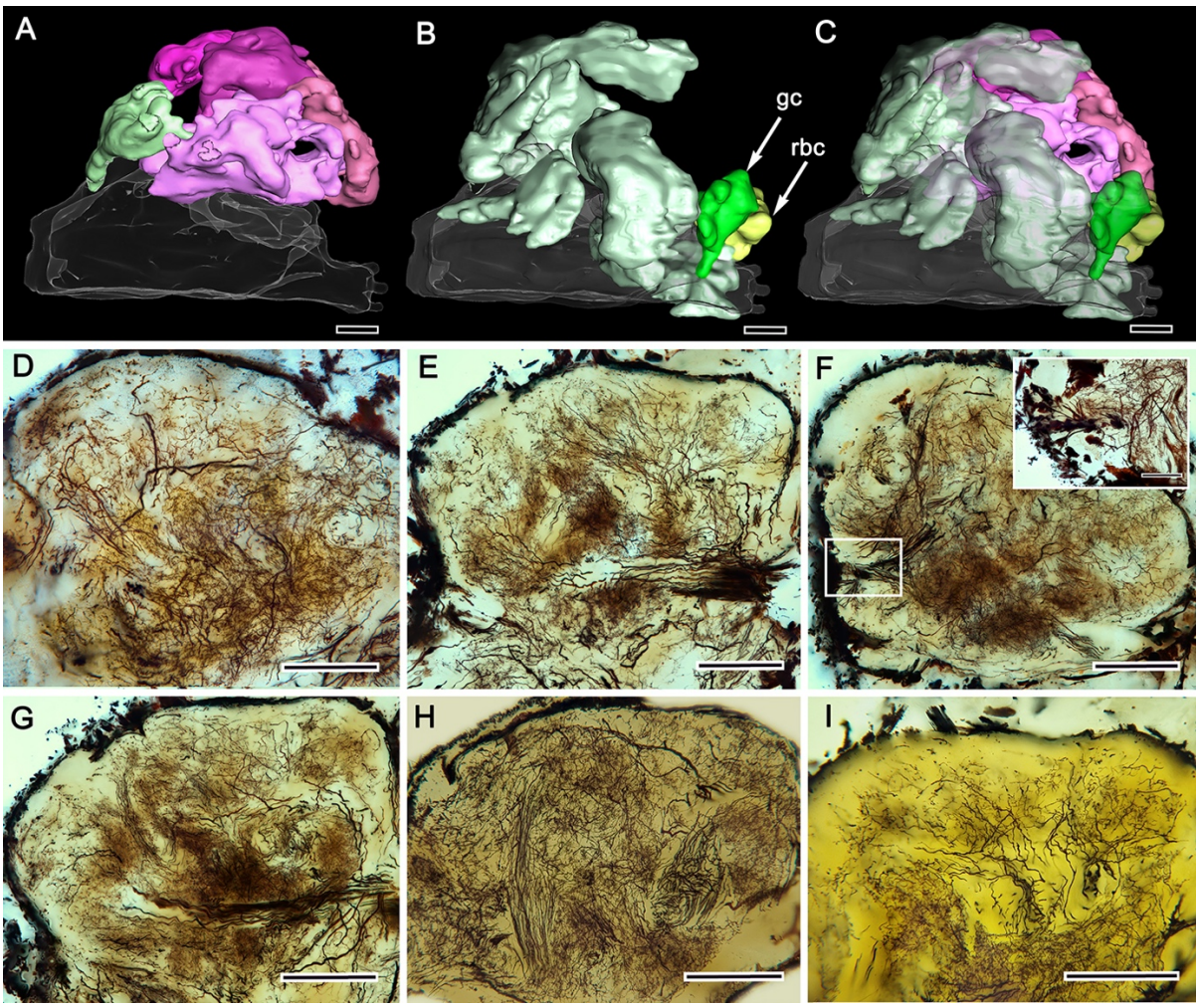

Figure 9 —— figure supplement 1. Perikaryal distributions and gyri neurons. (**A–C**). Amira-generated 3-D reconstruction of the gyri in panel A with the proximal gyrus (light green) above the medial root of the eyestalk nerve. Panel B shows extensive patches of neuronal perikarya, with the globuli cell cluster (gc, dark green) and reniform body cluster (rbc, yellow) situated at the distal margin of the RLPR. Merged images in panel C show the relative dispositions of cell body clusters and gyri. (**D-I**) Stitched reconstructions of Golgi mass impregnations resolve top (rostral)-down (F, H), lateral (E, G, I) and sub-gyrus (D) views of neuropils. The boxed area in F includes cell bodies of a lateral patch, enlarged in the upper right inset. Scale bars, A-I, 100μm, inset to panel F, 25μm.

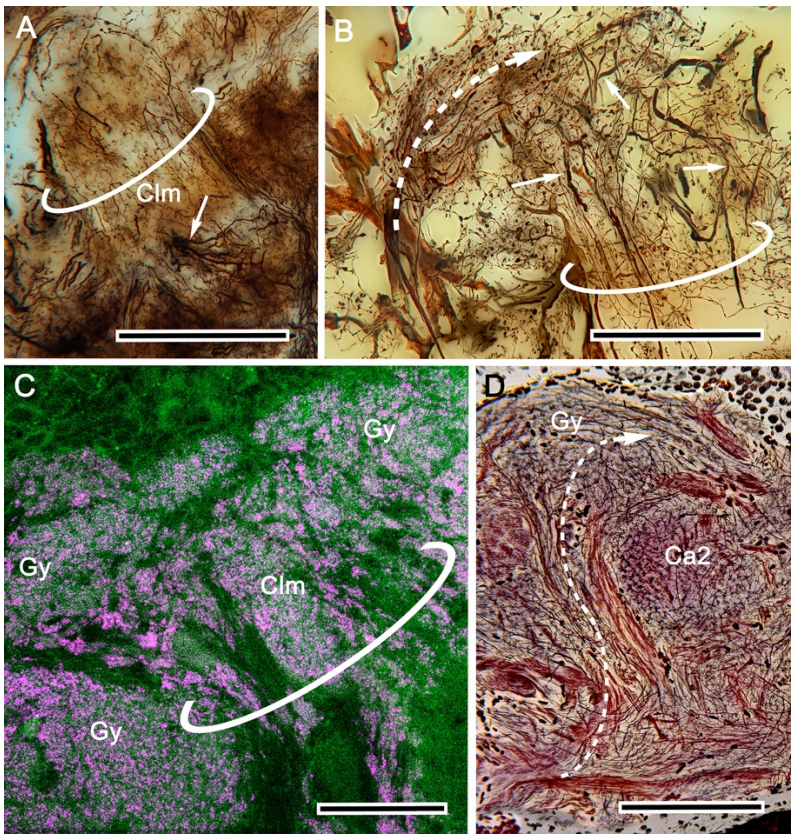

Figure 10 —— figure supplement 1. Column-gyrus interface organization**.** (**A**) Terminus of column 2 from calyx 2 (Clm, circled). The column is notable for its many extremely slender intrinsic processes. Also, visible in this preparation are branches of extrinsic (efferent) neurons extending across the column (arrow). (**B**) Terminus of column 2 (circled) with bundled intrinsic processes and the stouter profiles of efferent neurons (arrowed) ascending from the column into overlying gyral neuropil. This superficial level also receives terminals decorated with small bead-like specializations provided by bundled small-diameter axons from the eyestalk nerve (curved arrow). (**C**) Synapsin (magenta)-actin (green) labelling showing at the terminus of a column (circled) its longitudinal divisions denoted by various sizes and densities of synaptic sites across its width. Similar variation is resolved in flanking neuropil of the gyrus (Gy). (**D**) Reduced silver demonstrates bundles (dashed arrow) from the CLPR ascending outside a column into gyri, demonstrating that multimodal convergence occurs at many levels in the lateral protocerebrum. Part of Ca2 is also visible at this level. Scale bars**,** A, D, 100μm; B, 50μm; C, 25μm.

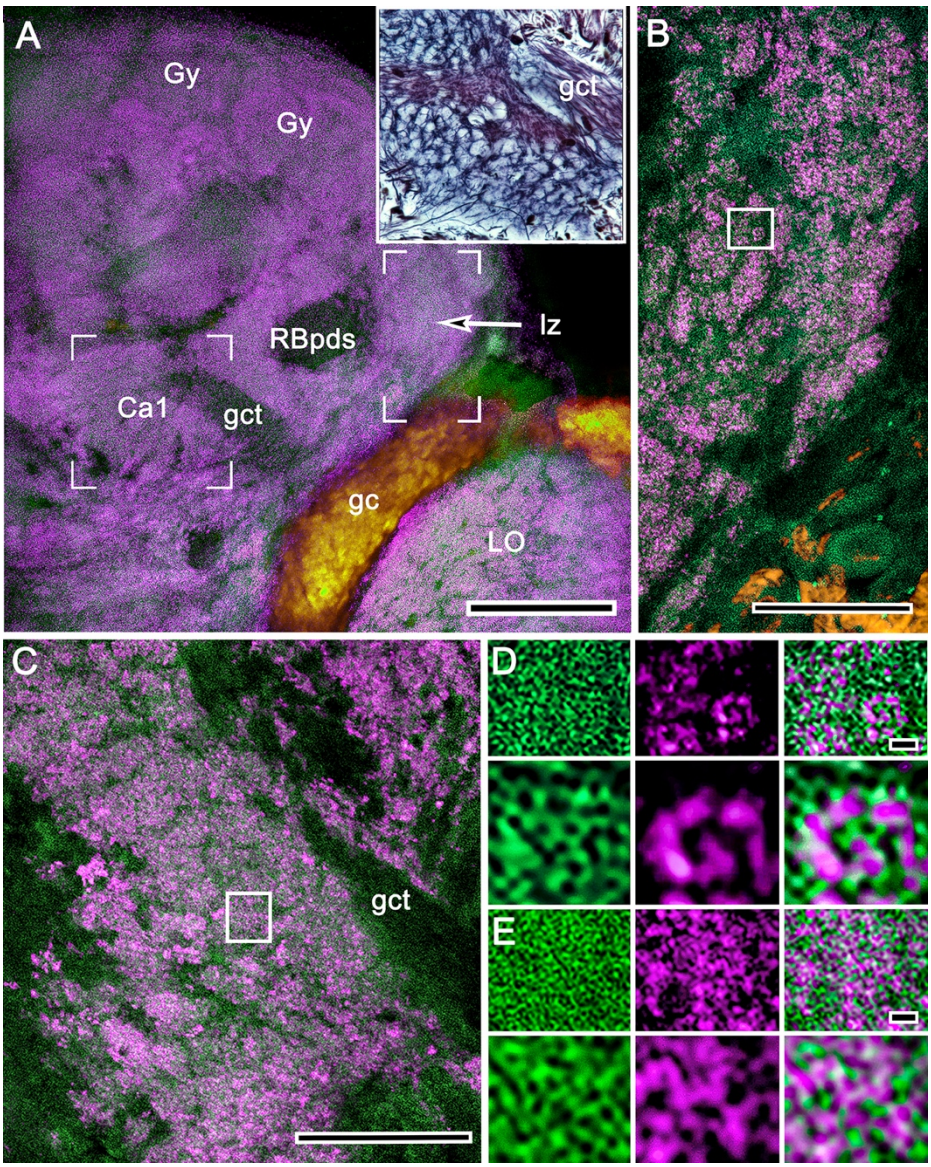

Figure 11 —— figure supplement 1. Comparison of synaptic densities associated with the calyces and reniform body. (**A**) Calyx 1 (Ca1), its associated gyri (Gy), the reniform body pedestal (RBpds) and, at this level, its lateral zone (lz) are shown labelled with actin (green)/anti-synapsin (magenta). In A, the open square corresponds to a similar area of silver-stained microglomeruli (upper right inset). The same area is shown enlarged in panel C. The open rectangle in A is enlarged in B to the same scale as panel C. (**B**) Reniform body neuropils comprise synaptic configurations that contribute to large glomerulus-like islets. (**C**) Microglomeruli of the calyces are smaller and more densely packed than those of the reniform body. (**D, E**) Comparison of synapsin/actin contributions to glomerulus-like units of the reniform body (D) and to microglomeruli of the mushroom body calyx (E) further demonstrates major differences regarding the density of their converging presynaptic elements. Other abbreviations: LO, lobula; gc, globuli cells; gct, globuli cell tract. Scale bars**,** A, 100μm; B,C, 25μm; D, E, 1μm.